Cell Reports

Gasdermin D pore-forming activity is redox-sensitive

Graphical abstract

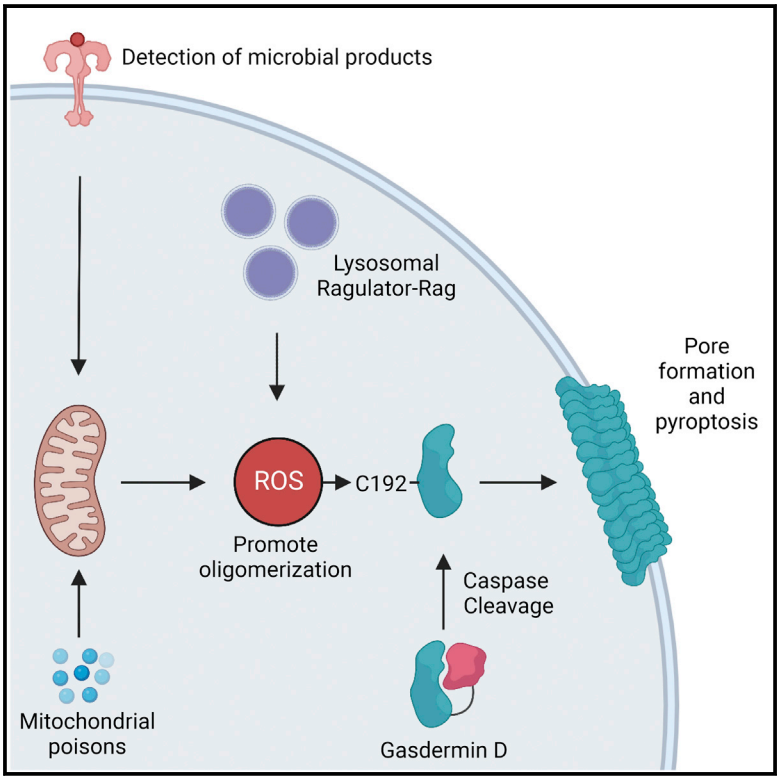

Highlights

- Reactive oxygen species (ROS) promote oligomerization of GSDMD and pyroptosis
- ROS induction can overcome pyroptosis defects in Ragulator-Rag-deficient cells
- Several cysteine residues in GSDMD become oxidized during pyroptosis
- Cys192 in GSDMD is necessary and sufficient for ROS responsiveness

Authors

Pascal Devant, Elvira Boršić, Elsy M. Ngwa, ..., Iva Hafner-Bratkovič, Charles L. Evavold, Jonathan C. Kagan

Correspondence

jay.thiagarajah@childrens.harvard.edu (J.R.T.), iva.hafner@ki.si (I.H.-B.), cevavold@mgh.harvard.edu (C.L.E.), jonathan.kagan@childrens.harvard.edu (J.C.K.)

In brief

Devant et al. investigate the actions of reactive oxygen species on the pore-forming protein GSDMD. They show that oxidation of a specific cysteine in GSDMD (C192) promotes its oligomerization, pore-forming activity, and pyroptosis. These findings reveal GSDMD as a redox-regulated protein that connects cellular redox state to inflammatory cell death.

Devant et al., 2023, Cell Reports *42*, 112008
January 31, 2023
https://doi.org/10.1016/j.celrep.2023.112008

CellPress

Cell Reports

CellPress
OPEN ACCESS

Report

Gasdermin D pore-forming activity is redox-sensitive

Pascal Devant,[1,8] Elvira Boršić,[2,3,8] Elsy M. Ngwa,[1,8] Haopeng Xiao,[5,6] Edward T. Chouchani,[5,6] Jay R. Thiagarajah,[1,*] Iva Hafner-Bratkovič,[2,4,*] Charles L. Evavold,[7,*] and Jonathan C. Kagan[1,9,*]

[1]Division of Gastroenterology, Boston Children's Hospital and Harvard Medical School, 300 Longwood Avenue, Boston, MA 02115, USA
[2]Department of Synthetic Biology and Immunology, National Institute of Chemistry, Hajdrihova 19, 1000 Ljubljana, Slovenia
[3]Graduate School of Biomedicine, University of Ljubljana, Kongresni trg 12, 1000 Ljubljana, Slovenia
[4]EN-FIST Centre of Excellence, Trg Osvobodilne fronte 13, 1000 Ljubljana, Slovenia
[5]Department of Cancer Biology, Dana-Farber Cancer Institute, Boston, MA, USA
[6]Department of Cell Biology, Harvard Medical School, Boston, MA, USA
[7]Ragon Institute of MGH, MIT and Harvard, 400 Technology Square, Cambridge, MA 02139, USA
[8]These authors contributed equally
[9]Lead contact
*Correspondence: jay.thiagarajah@childrens.harvard.edu (J.R.T.), iva.hafner@ki.si (I.H.-B.), cevavold@mgh.harvard.edu (C.L.E.), jonathan.kagan@childrens.harvard.edu (J.C.K.)
https://doi.org/10.1016/j.celrep.2023.112008

SUMMARY

Reactive oxygen species (ROS) regulate the activities of inflammasomes, which are innate immune signaling organelles that induce pyroptosis. The mechanisms by which ROS control inflammasome activities are unclear and may be multifaceted. Herein, we report that the protein gasdermin D (GSDMD), which forms membrane pores upon cleavage by inflammasome-associated caspases, is a direct target of ROS. Exogenous and endogenous sources of ROS, and ROS-inducing stimuli that prime cells for pyroptosis induction, promote oligomerization of cleaved GSDMD, leading to membrane rupture and cell death. We find that ROS enhance GSDMD activities through oxidative modification of cysteine 192 (C192). Within macrophages, GSDMD mutants lacking C192 show impaired ability to form membrane pores and induce pyroptosis. Reciprocal mutagenesis studies reveal that C192 is the only cysteine within GSDMD that mediates ROS responsiveness. Cellular redox state is therefore a key determinant of GSDMD activities.

INTRODUCTION

Reactive oxygen species (ROS) are produced by multiple mechanisms within cells, ranging from enzymatic activities to byproducts of aerobic respiration.[1] ROS can covalently modify proteins, DNA, and other biological molecules. The unregulated production of high amounts of ROS can be destructive to cells, as oxidized membranes may lose barrier function, oxidized DNA can result in mutation, and oxidized proteins can display altered biochemical activities. ROS include unstable short-lived molecules such as superoxide and hydroxyl free radicals as well as more stable forms such as hydrogen peroxide. In extreme situations, such as following ionizing radiation, ROS can alter cellular behaviors in such catastrophic ways that lysis occurs.[2] However, ROS also serve regulatory functions through modifications of proteins, DNA, or membranes that alter signaling activities and cellular behaviors.[3] Numerous examples of the influence of redox signaling have emerged, in particular in the context of environmental and inflammatory responses.[4,5]

Among the inflammatory mediators controlled by ROS is the interleukin-1 (IL-1) family of cytokines. IL-1β, the best-characterized member of this family, is most commonly released from cells through the actions of the protein gasdermin D (GSDMD).[6,7] GSDMD forms pores in the plasma membrane that can lead to a lytic form of cell death known as pyroptosis.[8] GSDMD and IL-1β are both synthesized as inactive pro-proteins that must be cleaved to achieve pore-forming abilities or inflammatory activities, respectively.[9–11] These cleavage events can be mediated by caspase-1, the principal enzymatic component of a large multiprotein complex called inflammasome.[12] Inflammasomes are not present within resting cells but are assembled upon cellular encounters with infectious or non-infectious threats to the host. The mechanisms by which inflammasomes are assembled have been the subject of intense investigation, with ROS being one of the first identified regulators of this process. Tschopp and colleagues recognized this link when they found that mitochondrial poisons that disrupt the electron transport chain (ETC) and induce ROS production can promote the assembly of inflammasomes containing the protein NLRP3.[13] In addition, more recent work has illustrated that microbial detection by Toll-like receptors (TLRs) can lead to ROS production from mitochondria, which amplifies the expression of the genes encoding NLRP3 and IL-1β and positions NLRP3 and caspase-1 on these

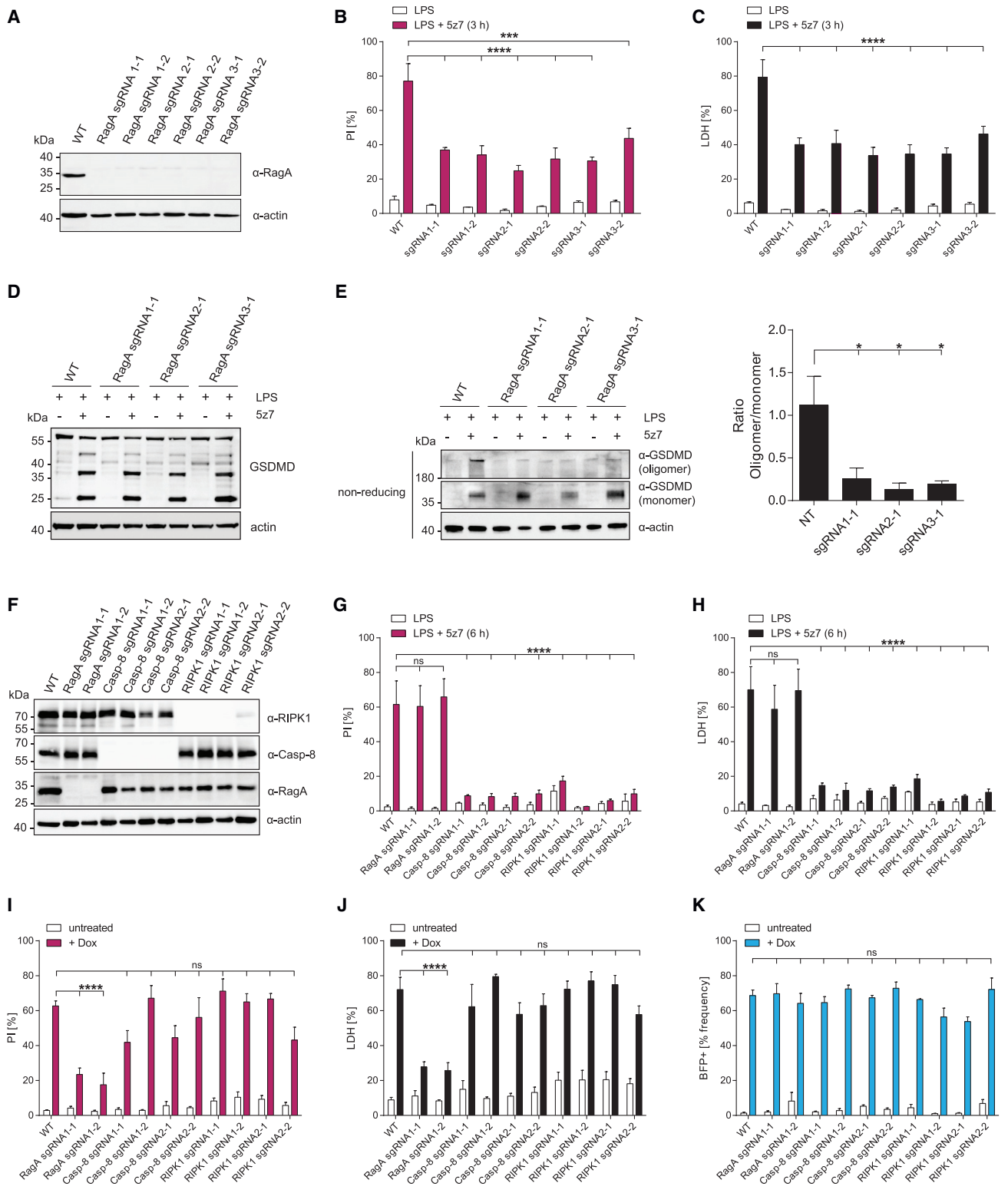

Figure 1. Dox-induced expression of NT-GSDMD leads to RIPK1- and caspase-8-independent pyroptosis

(A) Immunoblot analysis of RagA-deficient iBMDM clonal cell lines.

(B–E) RagA-deficient iBMDM or non-target sgRNA (WT) control cells were treated with LPS (1 μg/mL) alone or co-treated with LPS (1 μg/mL) and the TAK1 inhibitor 5z7 (250 nM) for 3 h. PI fluorescence and LDH release were quantified as a measure of membrane disruption/lysis (B and C). GSDMD processing and oligomerization were assessed by immunoblot under reducing (D) or non-reducing (E) conditions.

(legend continued on next page)

organelles.[14–16] Based on these studies, the prevailing concept is that ROS act at the apex of inflammasome pathways to regulate their function. However, whether and how ROS act at other stages of pyroptosis pathways remains undefined.

We recently identified the Ragulator-Rag complex, which is best known for its control of cellular metabolism, as a positive regulator of GSDMD-mediated cell death.[17] We found that GSDMD oligomerization into membrane pores that induce pyroptosis was defective in macrophages that lack the Ragulator-Rag components RagA or RagC. A link to ROS regulation was suggested, as defects in GSDMD pore-forming activity in RagA- or RagC-deficient cells could be rescued by the supply of exogenous ROS or induction of endogenous ROS from mitochondria. Incidentally, another study also reported a role for Ragulator-Rag in pyroptosis.[18] While both studies used genome-wide genetic screens to identify regulators of GSDMD-mediated pyroptosis, the experimental systems were different. The latter report studied a pathway that is induced when TLRs are activated concomitantly with inhibitors of the kinase TAK1, leading to caspase-8- and GSDMD-dependent pyroptosis. In contrast, our study used a reductionist system whereby macrophages were engineered to contain a doxycycline (Dox)-inducible transgene encoding the pore-forming domain of GSDMD (known as NT-GSDMD). Thus, whereas our study bypassed upstream regulatory events that lead to GSDMD cleavage and pore formation, the study by Zheng and colleagues[18] stimulated proteins that act upstream of GSDMD.

Herein, we sought to better define the role of Ragulator-Rag and ROS in the regulation of GSDMD activities. We used our Dox-inducible NT-GSDMD system to focus our studies on the terminal events in pyroptosis. Moreover, to further enable our studies, we used a version of GSDMD that contains an I105N mutation. NT-GSDMD I105N retains the ability to form membrane pores but does so more slowly than its wild-type (WT) counterpart.[9,19] This variant allowed for an increased window of time to study GSDMD through microscopy and biochemical analysis prior to cell rupture. Our studies revealed that under steady-state conditions, Ragulator-Rag is required for basal ROS production within cells that enables NT-GSDMD oligomerization and pyroptosis. Diverse immune signaling pathways or environmental perturbations that induce ROS can bypass the requirement of Ragulator-Rag and promote NT-GSDMD oligomerization and pore formation. Finally, we found that GSDMD is directly oxidized at multiple cysteine residues, with cysteine 192 (C192) being necessary and sufficient for ROS-mediated potentiation of GSDMD pore formation and pyroptosis. These findings reveal GSDMD as a redox-regulated protein that directly connects cellular redox state to inflammatory cell death via pyroptosis.

RESULTS

The two studies characterizing Ragulator-Rag in pyroptosis focused on distinct subunits of this protein complex. To compare the findings that were made, we created a common set of genetic tools and performed assays using pyroptosis stimuli that had been previously used in each of these studies.[17,18] We generated immortalized murine bone marrow-derived macrophages (iBMDMs) deficient for the Ragulator-Rag component RagA, the central GTPase that controls Ragulator functions. We electroporated Cas9-expressing iBMDMs with three different single guide RNAs (sgRNAs) targeting *Rraga*, the gene encoding RagA. Complete ablation of the RagA protein was observed in the resulting clonal iBMDM lines (Figure 1A). These cells were co-stimulated with the TLR4 ligand bacterial lipopolysaccharide (LPS) and the chemical 5z7, an inhibitor of TAK1. This treatment has been used to stimulate RIPK1- and caspase-8-mediated pyroptosis.[18,20] Pyroptosis was assessed by monitoring the release of the cytosolic enzyme lactate dehydrogenase (LDH) into the extracellular space. In addition, membrane permeabilization was assessed by staining cells with propidium iodide (PI), a membrane-impermeable dye that fluoresces upon binding intracellular nucleic acids. Cells that received a non-target control sgRNA (referred to as WT) stained strongly for PI and released LDH after LPS+5z7 treatment (Figures 1B and 1C). In contrast, RagA-deficient cells were protected from pyroptosis induction using both of these assays (Figures 1B and 1C). Processing of GSDMD was unchanged in RagA-deficient cells compared with WT cells, but we observed a decrease in GSDMD oligomer formation (Figures 1D, 1E, and S1A). Thus, similar to studies focused on other components of the Ragulator-Rag complex,[18] our results suggest that RagA is required for pyroptosis induced by LPS+5z7, but the underlying mechanism may vary depending on the specific Ragulator-Rag component.

We considered these findings in the context of our recent discovery that RagA was required for pyroptosis induced by the Dox-mediated expression of NT-GSDMD I105N, hereafter referred to as NT-GSDMD.[17] It was possible that Dox may stimulate RIPK1 and caspase-8, leading to NT-GSDMD-mediated pore formation. If this possibility was correct, impairing the function of RIPK1 or caspase-8 should lead to decreased pyroptosis upon Dox induction of NT-GSDMD. We first tested this hypothesis using small-molecule inhibitors. We Dox-induced NT-GSDMD in the presence of chemical inhibitors of RIPK1 (7-Cl-O-Nec-1), the related kinase RIPK3 (GSK'872), or the pan-caspase inhibitor zVAD. None of the inhibitors had a significant effect on Dox-induced cell death, as indicated by LDH release (Figure S1B). The inhibitor concentrations used in this analysis were functional, as we confirmed that these concentrations

(F) Immunoblot analysis of RagA-, caspase-8-, or RIPK1-deficient iBMDMs expressing NT-GSDMD under Dox-inducible promoter.
(G and H) RagA-, caspase-8-, or RIPK1-deficient iBMDMs expressing NT-GSDMD under Dox-inducible promoter were treated with LPS (1 μg/mL) alone or co-treated with LPS and the TAK1 inhibitor 5z7 (250 nM) for 6 h. PI fluorescence and LDH release were quantified as measure of membrane disruption/lysis.
(I–K) RagA-, caspase-8-, or RIPK1-deficient iBMDMs iBMDMs expressing NT-GSDMD under Dox-inducible promoter were treated with Dox (0.5 μg/mL) for 16 h. PI fluorescence and LDH release were quantified as measure of membrane disruption/lysis. Fraction of BFP-positive cells was measured by flow cytometry. Cells indicated as WT were electroporated with a non-targeting sgRNA. Data are mean ± SEM of three experiments. Immunoblots show representative result of three repeats. Statistical significance was determined by two-way ANOVA: *$p < 0.05$; **$p < 0.01$; ***$p < 0.001$; ****$p < 0.0001$.

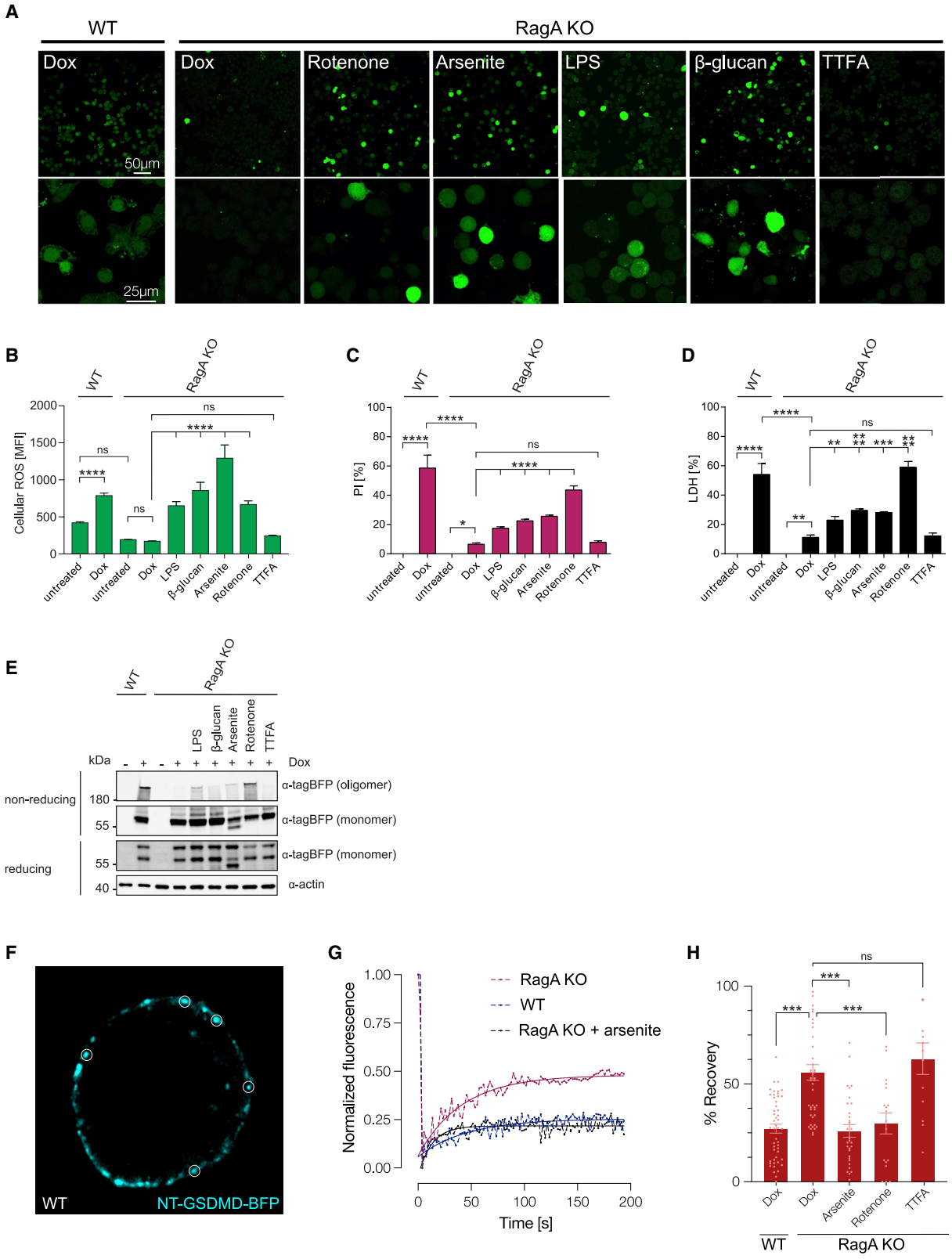

(legend on next page)

of 7-CL-O-Nec-1 inhibited LPS+5z7-induced pyroptosis (Figures S1C and S1D). Furthermore, GSK'872 inhibited LPS + zVAD-induced necroptosis, and zVAD inhibited GSDMD cleavage in LPS+5z7-treated cells (Figure S1C–S1E). To corroborate these findings, we generated cells lacking the genes encoding caspase-8 or RIPK1 (Figure 1F). We functionally confirmed RIPK1 and caspase-8 deficiencies, as the cells lacking these proteins were protected from LPS+5z7-induced pyroptosis, even after treatments of up to 6 h (Figures 1G and 1H). Interestingly, at this late time point, RagA-deficient cells died to a similar extent as WT cells (Figures 1G, 1H, and S1F). These results indicate that RIPK1 and caspase-8 are required for LPS+5z7-induced cell death at all time points examined, whereas RagA is most important for the rapid pyroptotic response induced by LPS+5z7. Similar to the findings made with chemical inhibitors, neither caspase-8 nor RIPK1 deficiencies impacted the PI staining or LDH release that was observed upon expression of NT-GSDMD (Figures 1I and 1J). In contrast, RagA-deficient cells were protected from cell death under the same conditions (Figures 1I and 1J). Using the BFP-tag that is appended to the C-terminus of NT-GSDMD, we verified that the frequency of BFP-positive cells was unchanged under all experimental conditions (Figure 1K). These collective findings indicate that RagA is required for pyroptosis in response to both LPS+5z7 treatments and Dox-induced expression of NT-GSDMD.

The common node in the pyroptotic events induced by LPS+5z7 and Dox treatments is GSDMD, suggesting that RagA acts at this stage in the pathway. To address the functions of GSDMD specifically, our subsequent work used the Dox-inducible system for NT-GSDMD activities. To better understand the link between RagA and GSDMD, we focused on the role of Ragulator-Rag in ROS regulation. We assembled a panel of agents that increase cellular ROS in distinct manners. This panel consists of two microbial products, LPS and fungal β-glucans, the environmental toxin sodium arsenite, and two mitochondrial ETC inhibitors, rotenone and TTFA.[21–23] Rotenone is an ROS fluxing agent, whereas treatment with TTFA is not expected to increase cellular ROS.[13] Live-cell confocal microscopy was used to assess ROS production by staining with the redox-sensitive fluorescent probe CM-H_2DCFDA. We found that treatment with Dox to induce NT-GSDMD expression led to an increase in cellular ROS in WT cells, but not in RagA-deficient cells (Figures 2A and 2B). Treatments of cells with LPS, β-glucan, sodium arsenite, or rotenone induced ROS in RagA-deficient cells, whereas TTFA did not (Figures 2A and 2B). Based on the ability of these agents to bypass the ROS production defects of RagA-deficient cells, we examined their ability to rescue defects in NT-GSDMD oligomer formation, PI staining, and LDH release. Dox induction of NT-GSDMD led to an increase in PI staining and LDH release in WT cells, which was reduced in RagA-deficient cells (Figures 2C and 2D). Interestingly, all the agents that rescued the ROS production defects in RagA-deficient cells (LPS, β-glucan, sodium arsenite, rotenone) also rescued PI staining and LDH release defects in these cells (Figures 2C and 2D). Importantly, the rescue of PI staining and LDH release was accompanied by an increase in GSDMD oligomerization (Figure 2E).[8] When we co-treated WT cells with Dox and the same panel of compounds, we observed accelerated plasma membrane perforation compared with cells treated with Dox alone (Figure S2A). In the absence of NT-GSDMD, these compounds did not affect membrane permeability (Figure S2B). The strongest ROS inducers (rotenone, sodium arsenite) exhibited the strongest acceleration of plasma membrane perforation (Figure S2A). These data demonstrate that a diverse array of ROS-fluxing stimuli, including those that are commonly used to prime cells for inflammasome responsiveness, are capable of restoring GSDMD pore formation and pyroptosis in RagA-deficient cells and enhancing these processes in WT cells.

To complement the biochemical analysis of ROS-induced GSDMD oligomer formation, we examined oligomerization of GSDMD within individual cells *in situ* by fluorescence recovery after photo bleaching (FRAP) on BFP-tagged NT-GSDMD. Following induction of NT-GSDMD-BFP in RagA-deficient or WT cells, we targeted membrane-localized BFP fluorescence areas for photobleaching and monitored subsequent fluorescence recovery (Figures 2F and 2G). Multimerization of a membrane-bound protein into a larger complex leads to reduced two-dimensional diffusion, as compared with monomers. This reduced diffusion leads to longer fluorescence recovery times following photobleaching, as well as a reduction in the total mobile fraction or percent recovery over the timescale of the experiment.[24] Consistent with this notion, RagA-deficient cells, where GSDMD oligomerization is impaired, exhibited an increased mobile fraction compared with WT cells (Figures 2G and 2H). Consistent with our biochemical analyses, treatment with ROS-inducing agents rotenone or sodium arsenite reduced the percent recovery in RagA-deficient cells (Figures 2G and 2H). In contrast, TTFA did not alter fluorescence recovery of NT-GSDMD in RagA-deficient cells (Figure 2H). These experiments in live macrophages support the conclusion that ROS control

Figure 2. Priming with microbial products or environmental toxins induces ROS and promotes GSDMD pore formation

RagA-deficient or WT iBMDMs expressing NT-GSDMD under Dox-inducible promoter were treated with Dox (2 μg/mL in A, B, E or 0.5 μg/mL in C, D) for 8 h. PAMPs (1 μg/mL of LPS; 1 mg/mL of β-glucan) were present throughout the entire stimulation period. Toxins (20 μM sodium arsenite; 5 μM rotenone; 100 μM TTFA) were added after 4 h.

(A and B) Cells were stained using the ROS-reactive dye CM-H2DCFDA and signal was quantified by fluorescence microscopy.

(C and D) PI fluorescence and LDH release were quantified as measure of membrane disruption/lysis.

(E) GSDMD oligomerization was assessed by immunoblot under non-reducing conditions.

(F) Representative confocal image of WT cell after Dox induction of NT-GSDMD-BFP for 8 h. Circles indicate areas for measurement of FRAP.

(G) Representative FRAP curves from WT cells, and RagA-deficient cells co-treated with sodium arsenite.

(H) Mean proportion of FRAP of NT-GSDMD-BFP signal in WT and RagA-deficient iBMDMs after Dox induction (2 μg/mL) for 8 h. Arsenite (20 μM), Rotenone (5 μM), or TTFA (100 μM) were added after 4 h. Cells indicated as WT were transduced with an empty vector. Data are mean ± SEM of at least three experiments. Immunoblots and microscopy images show representative result of three repeats. Statistical significance was determined by one-way ANOVA (B–D) or two-way ANOVA with Tukey's or Dunnett's post hoc testing (H): *$p < 0.05$; **$p < 0.01$; ***$p < 0.001$; ****$p < 0.0001$.

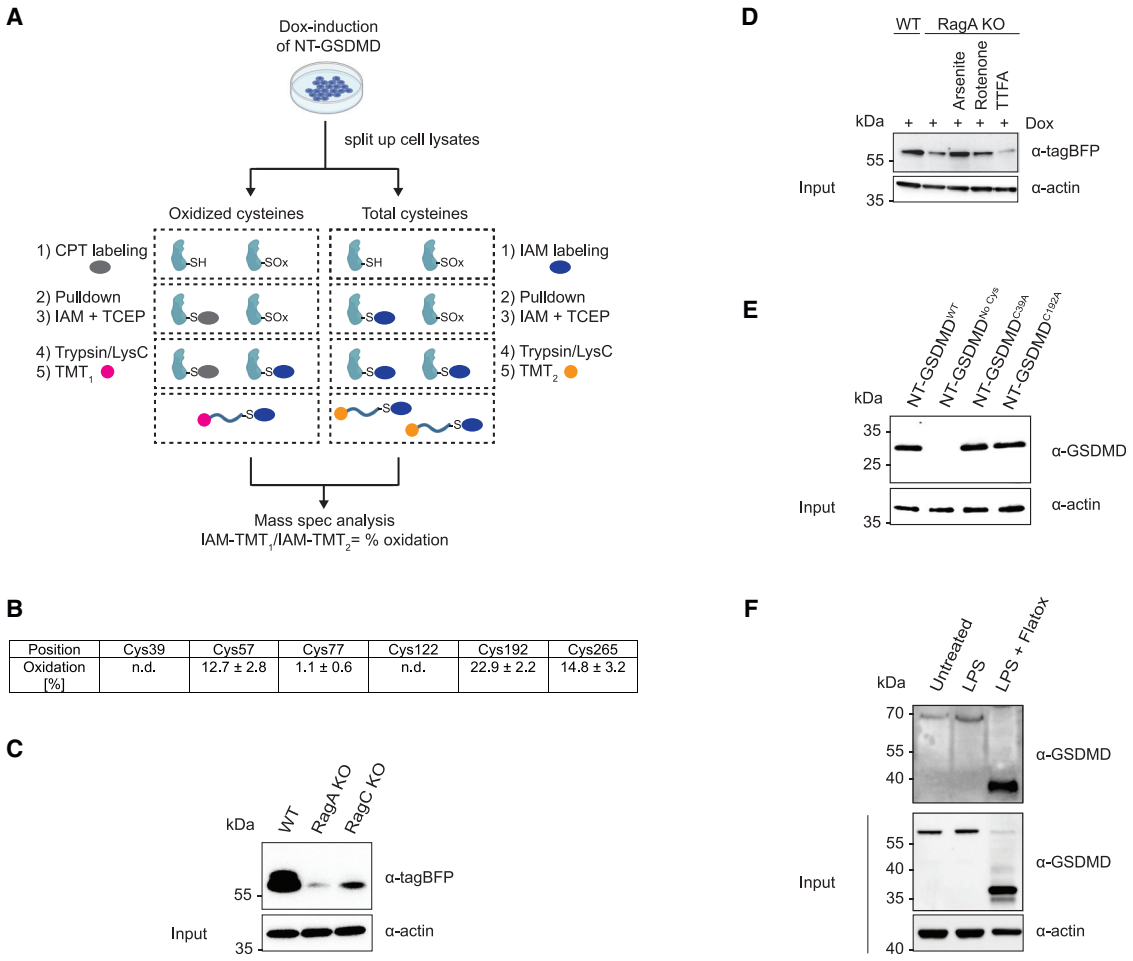

Figure 3. NT-GSDMD is oxidized upon pyroptosis induction in a RagA-dependent manner

(A) Schematic of proteomics approach to determine absolute cysteine oxidation. CPT, cysteine-reactive phosphate tag; IAM, iodoacetamide; TMT, tandem mass tag.

(B) Quantitative mass spectrometry analysis of oxidative state of cysteine residues in NT-GSDMD. iBMDMs expressing NT-GSDMD-BFP under Dox-inducible promoter were treated with 2 μg/mL Dox for 8 h. n.d. indicates that no peptides containing this cysteine residue were detected and oxidative state could therefore not be determined.

(C and D) Pulldown and immunoblot analyses to assess relative cysteine oxidation in RagA- or RagC-deficient, or empty-vector-treated iBMDMs (WT) expressing NT-GSDMD-BFP under Dox-inducible promoter. Cells were treated with Dox (2 μg/mL) for 8 h. Toxins (20 μM sodium arsenite; 5 μM rotenone; 100 μM TTFA) were added after 4 h.

(E) Pulldown and immunoblot analyses to assess relative cysteine oxidation in GSDMD KO iBMDMs expressing indicated NT-GSDMD mutants under Dox-inducible promoter. Cells were treated with Dox (2 μg/mL) for 8 h.

(F) Pulldown and immunoblot analyses to assess relative cysteine oxidation in WT iBMDMs. Cells were primed with LPS (1 μg/mL) for 4 h or left unprimed before stimulation with Flatox for 2 h. Data presented in (E) were generated using a bulk population of cells. Data in (B) are represented as mean ± SEM of four independent repeats. Immunoblots show representative result of three (C–E) or two (F) independent repeats.

GSDMD oligomerization and pore formation within the plasma membrane.

Redox-regulation of proteins often occurs via direct modification of thiol-containing amino acid residues such as cysteines. A possible mechanism for ROS-mediated GSDMD pore regulation would be direct oxidation of cysteine residues within NT-GSDMD. We therefore investigated whether any cysteines in NT-GSDMD are oxidized during pyroptosis. We determined the absolute fraction of oxidation for four out of six cysteines in NT-GSDMD (C57, C77, C192, C265) following Dox induction using a mass spectrometry-based approach that allows for the quantification of reversible oxidation of thiols (Figure 3A).[25] Absolute cysteine oxidation values varied between 1.1% (C55) and 22.9% (C192) (Figure 3B). These results suggest that C192 is oxidized during pyroptosis. To corroborate these results, we analyzed relative cysteine oxidation by pulling down oxidized cysteine (sulfenic acid) residues using a biotin-maleimide probe.[26] We detected a strong signal for GSDMD in WT cells upon Dox treatment (Figures 3C and S3A). This signal is diminished in RagA- or RagC-deficient cells, a finding consistent with lower basal and induced cellular ROS in the absence of Ragulator-Rag functions (Figures 3C, 2A, and 2B). When

CellPress
OPEN ACCESS

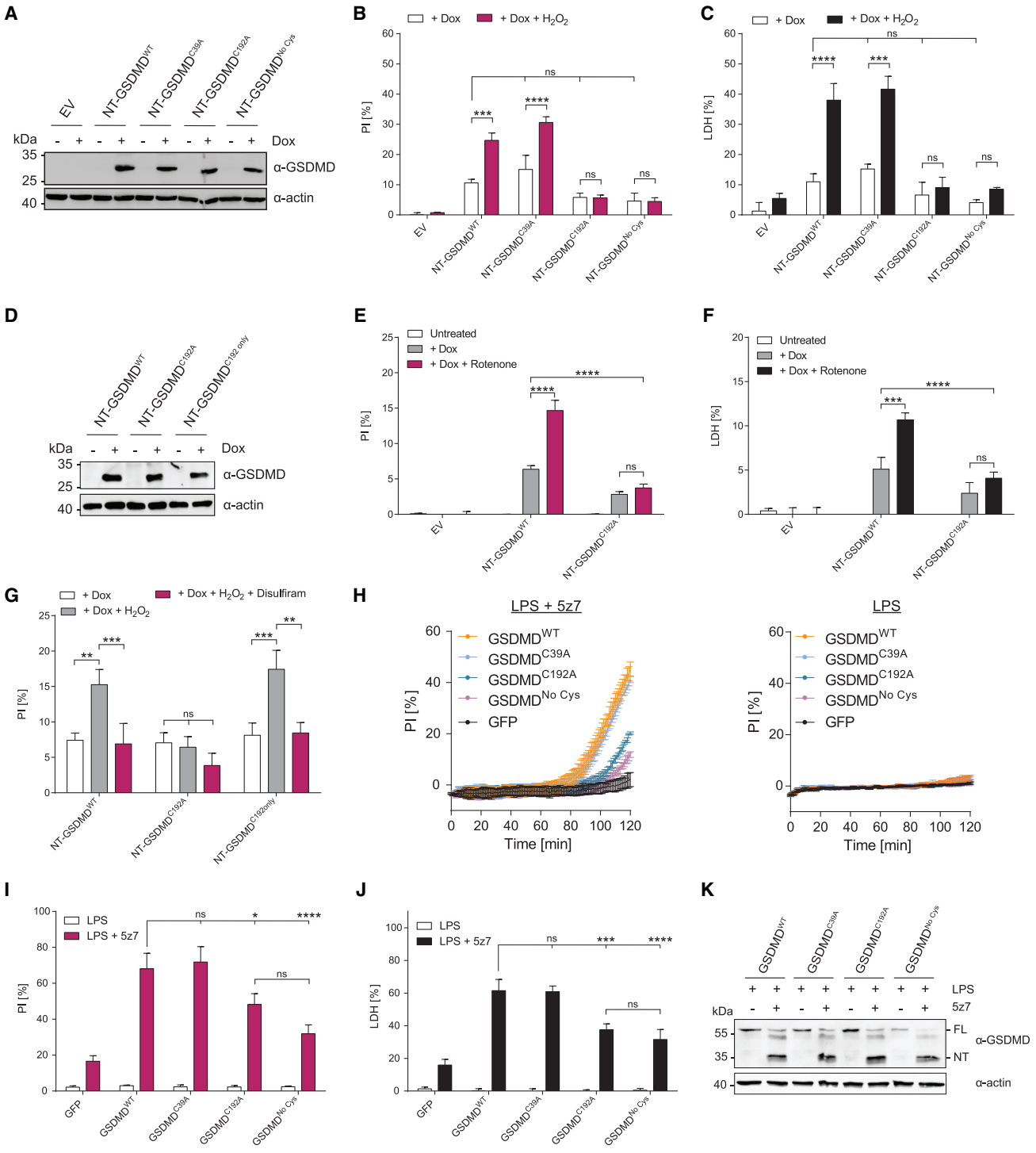

Figure 4. ROS-induced enhancement of pyroptosis is dependent on C192 in GSDMD

(A and D) Immunoblot analysis of whole-cell lysates of GSDMD KO iBMDM expressing indicated NT-GSDMD mutants under a Dox-inducible promoter or transduced with an empty vector (EV). Cells were treated with 1 μg/mL of Dox for 4 h or left untreated.

(B, C, and G) GSDMD KO iBMDMs expressing indicated NT-GSDMD variants under a Dox-inducible promoter or transduced with an empty vector (EV) were treated with Dox (1 μg/mL) for 8 h. DMSO or disulfiram was added after 4 h to a final concentration 25 μM (G). H_2O_2 was added after 6 h to a final concentration of 625 μM. PI fluorescence and LDH release were quantified as a measure of membrane disruption/lysis (B and C).

(legend continued on next page)

RagA-deficient cells were co-treated with the ROS-inducing agents rotenone or sodium arsenite, NT-GSDMD oxidation was partially restored (Figures 3D and S3B). Using this orthogonal pulldown assay, we confirmed that cysteine oxidation within NT-GSDMD can occur at multiple residues, as suggested by our mass spectrometry quantification. We observed no notable reduction in pulldown efficiency when examining C39A or C192A mutants (Figures 3E and S3C), likely due to sufficient cysteine oxidation on other residues (Figure 3B). Highlighting the on-target specificity of the pulldown assay, we observed complete loss of signal in the No Cys mutant, in which all cysteines were mutated to alanine (Figure 3E). Last, we performed a similar pulldown experiment in WT iBMDMs stimulated with the synthetic toxin Flatox, an inducer of NAIP/NLRC4 inflammasome-dependent pyroptosis.[27] In Flatox-treated cells, the oxidized cysteine pulldown assay identified cleaved NT-GSDMD, suggesting that endogenous NT-GSDMD becomes oxidized during pyroptosis (Figure 3F). Overall, these data indicate that GSDMD protein can detect ROS directly.

Next, we investigated whether oxidation of specific cysteine residues in NT-GSDMD affects its ability to form pores and induce cell death. If this was the case, mutation of cysteine to a non-oxidizable amino acid (e.g., alanine) should affect the ability of such mutant to form pores and induce cell death. Notably, several cysteines in the N-terminal domain of GSDMD, including C191/192 and C38/C39 in human/murine GSDMD, have been implicated in GSDMD oligomerization and pore formation.[8,28,29] To investigate the importance of these cysteine residues for GSDMD-mediated cell death, we engineered GSDMD-deficient iBMDMs to express NT-GSDMD carrying C39A or C192A mutations, or an NT-GSDMD variant where all six cysteines have been mutated to alanine (No Cys) under the control of a Dox-inducible promoter. Dox treatments led to the production of comparable amounts of all NT-GSDMD proteins (Figure 4A), but none of the mutant NT-GSDMD variants exhibited a decreased basal ability to induce pyroptosis (Figures 4B and 4C). Based on the suggested role of ROS in GSDMD pore formation, we determined if an additional supply with ROS, as would be the case during inflammasome priming, might reveal a phenotype in the context of cysteine substitution. To examine this possibility, we induced NT-GSDMD variants with Dox and provided exogenous ROS by co-treating cells with H_2O_2. Under these conditions, we observed an enhancement of pore-forming activities induced by WT NT-GSDMD and the C39A mutant (Figures 4B and 4C). In contrast, no ROS-mediated enhancement of PI staining or LDH release was observed in cells expressing the C192A or the No Cys mutant (Figures 4B and 4C). Similar results were obtained with cells expressing NT-GSDMD constructs lacking the I105N mutations or when mitochondrial ROS were triggered by rotenone (Figures S4A–S4C, 4E, and 4F). Interestingly, C192 was sufficient to enable ROS-mediated enhancement of pore formation. A boost in PI staining by H_2O_2 was observed in cells expressing an NT-GSDMD variant in which all cysteine residues were mutated to alanine except C192 (Figure 4G). This boost in PI signal was abrogated by the C192-targeting drug disulfiram (Figure 4G).[30] These findings support the role of ROS as a potentiator of GSDMD pore-forming activities and establish C192 as a necessary and sufficient regulator of these events.

To test the importance of C192 in response to a natural pyroptotic stimulus, we reconstituted GSDMD-deficient cells with full-length GSDMD variants carrying the above-described mutations (WT, C39A, C192A, No Cys; Figure S4D). We induced pyroptosis by LPS+5z7 treatment and monitored membrane permeabilization and cell death induction by PI staining and LDH assay. PI staining and LDH release, but not GSDMD cleavage, were impaired in cells expressing GSDMD C192A or the No Cys mutant compared with cells expressing WT GSDMD (Figures 4H–4K). Mutating C39 in GSDMD to alanine, on the other hand, had no effect on the kinetics of LPS+5z7-induced pyroptosis (Figures 4H–4K).

DISCUSSION

A central point that emerges from this study is that ROS can directly potentiate NT-GSDMD oligomerization, independently of upstream inflammasome effects. Based on the established role of ROS at the apex of the NLRP3 pathway and recent reports suggesting ROS-mediated regulation of the inflammasome adaptor protein ASC and the enzyme caspase-1,[13,31,32] we propose the idea of an ROS regulatory cascade, akin to phosphorylation cascades, where multiple nodes in a pathway are subject to the same type of regulation (ROS or phosphorylation; Figure S4E). This idea has important implications for the use of LPS and other innate immune agonists that flux ROS as priming agents to promote inflammasome activities.

We propose an additional role for the priming step in inflammasome activation (often referred to as signal 1). In addition to the invoked transcriptional changes (upregulation of inflammasome components and pro-IL-1β[15,16]), priming agents induce ROS that potentiate GSDMD oligomer formation and pyroptosis. Moreover, the common association of ROS with mitochondrial dysfunction and microbial infection suggests that ROS may act as a secondary messenger within host defense pathways to communicate threat level through regulation of distinct inflammasome-related proteins. As ROS metabolites may also negatively regulate catalytic cysteines within inflammatory caspases,

(E and F) GSDMD KO iBMDMs expressing indicated NT-GSDMD variants under a Dox-inducible promoter or transduced with an empty vector (EV) were treated with Dox (0.5 μg/mL) for 8 h. Rotenone was added after 4 h to a final concentration of 5 μM. PI fluorescence and LDH release were quantified as a measure of membrane disruption/lysis.

(H–K) GSDMD KO iBMDMs expressing indicated full-length GSDMD variants or GFP were treated with LPS (1 μg/mL) or co-treated with LPS (1 μg/mL) and the TAK1 inhibitor 5z7 (250 nM) for 2 h. LDH release and PI fluorescence was quantified in real time (H) or at the endpoint (I and J) to assess plasma membrane disruption. Processing of GSDMD was assessed by immunoblot (K). Data shown in (A)–(G) were generated using representative clonal cell populations. Clonal populations used were directly derived from bulk populations used in Figure 3E. Unless stated otherwise, data are mean ± SEM of at least three experiments, except for EV in (B) and (C), which is mean ± SEM of two experiments. Immunoblots show representative results of three repeats. PI curves are represented as mean ± SD of two technical replicates and representative of three repeats. Statistical significance was determined by two-way ANOVA with Tukey's post hoc testing: *p < 0.05; **p < 0.01; ***p < 0.001; ****p < 0.0001.

we expect that spatial and temporal consideration of ROS production will emerge in future studies as critical for pyroptotic signaling.[33]

Mechanistically, our finding that cysteines in NT-GSDMD are oxidized by ROS in a Rag-Ragulator-dependent manner is notable, as cysteine residues are known targets of several metabolite-based and small-molecule GSDMD inhibitors. For example, C192 is targeted by the cysteine-reactive inhibitors disulfiram, necrosulfamide, and dimethyl fumarate, highlighting that this residue is accessible for posttranslational modifications (PTMs).[28–30] Consistent with these reports, our analyses of GSDMD lacking C192 or all cysteine residues yielded a defect in LPS+5z7-mediated pyroptosis. Our functional analyses using Dox-induced NT-GSDMD carrying the same mutations revealed a necessary and sufficient role for C192 for potentiation of GSDMD pore-forming activities upon ROS stimulation. We do not expect a role for disulfide bonds, as this is inconsistent with the positioning of C192 in a recent high-resolution structure of oligomerized GSDMD.[34] We favor a model whereby ROS-mediated oxidation of cysteines aids the addition or removal of an activating or inhibitory PTM, respectively. Recent reports suggest that host metabolic states may modify GSDMD with an inhibitory mark.[29,35] Hence, our data may represent removal of an inhibitory mark on C192 in a subset of GSDMD molecules. Overall, we propose that GSDMD function is directly controlled by cellular redox state, a finding that provides a mandate to explore GSDMD cysteine oxidation as a biomarker of productive inflammasome activation.

Limitations of the study

While we mechanistically focus on the terminal step in the pyroptosis pathway, namely pore formation by the caspase cleavage fragment NT-GSDMD, it is likely that ROS can regulate distinct upstream steps within pyroptotic signaling. Further studies with natural stimulations and infections will allow us to assay the impact of ROS on other steps in the pathway. Consistent with this idea, a recent study reported a role for the Ragulator component Lamtor1 in NLRP3-dependent inflammasome activation.[36] We have not yet uncovered the specific mechanism by which cysteine oxidation mediates increased GSDMD pore formation and membrane permeability. In addition to a direct effect mediated by C192 in NT-GSDMD, we cannot rule out that there may be additional effects of ROS production that help membrane permeability, such as inhibition of autophagy or direct membrane oxidation.

STAR★METHODS

Detailed methods are provided in the online version of this paper and include the following:

- KEY RESOURCES TABLE
- RESOURCE AVAILABILITY
  - Lead contact
  - Materials availability
  - Data and code availability
- EXPERIMENTAL MODEL AND SUBJECT DETAILS
  - Cell culture
- METHOD DETAILS
  - Reagents and antibodies
  - Constructs
  - Cell lines
  - Generation of KO cell lines using CRISPR/Cas9 technology
  - GSDMD cleavage and oligomerization assay
  - Dox-induction of NT-GSDMD
  - Induction of caspase-8 and RIPK1-mediated pyroptosis by TAK1 inhibitor treatment
  - Propidium iodide staining and LDH assay
  - Pulldown of oxidized GSDMD
  - Fluorescence recovery after photo bleaching (FRAP)
  - ROS measurements
  - Proteomics
- QUANTIFICATION AND STATISTICAL ANALYSIS

SUPPLEMENTAL INFORMATION

Supplemental information can be found online at https://doi.org/10.1016/j.celrep.2023.112008.

ACKNOWLEDGMENTS

We thank all members of the Kagan lab for helpful discussions. This work was supported by NIH grants AI133524, AI093589, AI116550, and P30DK34854 to J.C.K. P.D. was supported by a scholarship by the Boehringer Ingelheim Fonds. C.L.E. was supported by a Ragon Early Independence Fellowship. I.H.-B. and E.B. acknowledge funding by the Slovenian Research Agency (ARRS grants J3-1746 and P4-0176 and young researcher grant). J.R.T. is supported by grants R03DK125630 (NIDDK) and R35GM142683 (NIGMS) and P30DK034854 (NIDDK). E.T.C. is supported by the Claudia Adams Barr Program, the Lavine Family Fund, the Pew Charitable Trust, NIH DK123095, and NIH AG071966. H.X. is supported by NIH grant K99AG073461.

AUTHOR CONTRIBUTIONS

Conceptualization: C.L.E., P.D., I.H.-B., and J.C.K.; methodology, P.D., E.M.N., E.B., C.L.E., I.H.-B., J.R.T., E.T.C., H.X., and J.C.K.; investigation, P.D., E.B., E.M.N., C.L.E., I.H.-B., and H.X.; visualization, P.D., E.B. C.L.E., I.H.-B., E.M.N., and J.R.T.; writing – original draft, P.D. and C.L.E.; writing – review & editing, all authors; funding acquisition, C.L.E., I.H.-B., P.D., A.H.S., J.R.T., E.T.C., H.X., and J.C.K.; supervision, C.L.E., I.H.-B., E.T.C., J.R.T., and J.C.K.

DECLARATION OF INTERESTS

J.C.K. consults and holds equity in Corner Therapeutics, Larkspur Biosciences, and Neumora Therapeutics. E.T.C. is co-founder, equity holder, and board member of Matchpoint Therapeutics and co-founder and equity holder in Aevum Therapeutics. None of these relationships influenced this study.

Received: April 23, 2022
Revised: November 21, 2022
Accepted: December 31, 2022

REFERENCES

1. Zorov, D.B., Juhaszova, M., and Sollott, S.J. (2014). Mitochondrial reactive oxygen species (ROS) and ROS-induced ROS release. Physiol. Rev. *94*, 909–950. https://doi.org/10.1152/physrev.00026.2013.
2. Juan, C.A., Pérez de la Lastra, J.M., Plou, F.J., and Pérez-Lebeña, E. (2021). The chemistry of reactive oxygen species (ROS) revisited: outlining their role in biological macromolecules (DNA, lipids and proteins) and

induced pathologies. Int. J. Mol. Sci. *22*, 4642. https://doi.org/10.3390/ijms22094642.

3. Sies, H., and Jones, D.P. (2020). Reactive oxygen species (ROS) as pleiotropic physiological signalling agents. Nat. Rev. Mol. Cell Biol. *21*, 363–383. https://doi.org/10.1038/s41580-020-0230-3.
4. Miller, G., Suzuki, N., Ciftci-Yilmaz, S., and Mittler, R. (2010). Reactive oxygen species homeostasis and signalling during drought and salinity stresses. Plant Cell Environ. *33*, 453–467. https://doi.org/10.1111/j.1365-3040.2009.02041.x.
5. Stottmeier, B., and Dick, T.P. (2016). Redox sensitivity of the MyD88 immune signaling adapter. Free Radic. Biol. Med. *101*, 93–101. https://doi.org/10.1016/j.freeradbiomed.2016.10.004.
6. Evavold, C.L., Ruan, J., Tan, Y., Xia, S., Wu, H., and Kagan, J.C. (2018). The pore-forming protein gasdermin D regulates interleukin-1 secretion from living macrophages. Immunity *48*, 35–44.e6. https://doi.org/10.1016/j.immuni.2017.11.013.
7. Heilig, R., Dick, M.S., Sborgi, L., Meunier, E., Hiller, S., and Broz, P. (2018). The Gasdermin-D pore acts as a conduit for IL-1β secretion in mice. Eur. J. Immunol. *48*, 584–592. https://doi.org/10.1002/eji.201747404.
8. Liu, X., Zhang, Z., Ruan, J., Pan, Y., Magupalli, V.G., Wu, H., and Lieberman, J. (2016). Inflammasome-activated gasdermin D causes pyroptosis by forming membrane pores. Nature *535*, 153–158. https://doi.org/10.1038/nature18629.
9. Kayagaki, N., Stowe, I.B., Lee, B.L., O'Rourke, K., Anderson, K., Warming, S., Cuellar, T., Haley, B., Roose-Girma, M., Phung, Q.T., et al. (2015). Caspase-11 cleaves gasdermin D for non-canonical inflammasome signalling. Nature *526*, 666–671. https://doi.org/10.1038/nature15541.
10. Shi, J., Zhao, Y., Wang, K., Shi, X., Wang, Y., Huang, H., Zhuang, Y., Cai, T., Wang, F., and Shao, F. (2015). Cleavage of GSDMD by inflammatory caspases determines pyroptotic cell death. Nature *526*, 660–665. https://doi.org/10.1038/nature15514.
11. Afonina, I.S., Müller, C., Martin, S.J., and Beyaert, R. (2015). Proteolytic processing of interleukin-1 family cytokines: variations on a common theme. Immunity *42*, 991–1004. https://doi.org/10.1016/j.immuni.2015.06.003.
12. Schroder, K., and Tschopp, J. (2010). The inflammasomes. Cell *140*, 821–832. https://doi.org/10.1016/j.cell.2010.01.040.
13. Zhou, R., Yazdi, A.S., Menu, P., and Tschopp, J. (2011). A role for mitochondria in NLRP3 inflammasome activation. Nature *469*, 221–225. https://doi.org/10.1038/nature09663.
14. West, A.P., Brodsky, I.E., Rahner, C., Woo, D.K., Erdjument-Bromage, H., Tempst, P., Walsh, M.C., Choi, Y., Shadel, G.S., and Ghosh, S. (2011). TLR signalling augments macrophage bactericidal activity through mitochondrial ROS. Nature *472*, 476–480. https://doi.org/10.1038/nature09973.
15. Iyer, S.S., He, Q., Janczy, J.R., Elliott, E.I., Zhong, Z., Olivier, A.K., Sadler, J.J., Knepper-Adrian, V., Han, R., Qiao, L., et al. (2013). Mitochondrial cardiolipin is required for Nlrp3 inflammasome activation. Immunity *39*, 311–323. https://doi.org/10.1016/j.immuni.2013.08.001.
16. Elliott, E.I., Miller, A.N., Banoth, B., Iyer, S.S., Stotland, A., Weiss, J.P., Gottlieb, R.A., Sutterwala, F.S., and Cassel, S.L. (2018). Cutting edge: mitochondrial assembly of the NLRP3 inflammasome complex is initiated at priming. J. Immunol. *200*, 3047–3052. https://doi.org/10.4049/jimmunol.1701723.
17. Evavold, C.L., Hafner-Bratkovič, I., Devant, P., D'Andrea, J.M., Ngwa, E.M., Boršić, E., Doench, J.G., LaFleur, M.W., Sharpe, A.H., Thiagarajah, J.R., and Kagan, J.C. (2021). Control of gasdermin D oligomerization and pyroptosis by the Ragulator-Rag-mTORC1 pathway. Cell *184*, 4495–4511.e19. https://doi.org/10.1016/j.cell.2021.06.028.
18. Zheng, Z., Deng, W., Bai, Y., Miao, R., Mei, S., Zhang, Z., Pan, Y., Wang, Y., Min, R., Deng, F., et al. (2021). The lysosomal Rag-Ragulator complex licenses RIPK1– and caspase-8–mediated pyroptosis by Yersinia. Science *372*, eabg0269. https://doi.org/10.1126/science.abg0269.
19. Aglietti, R.A., Estevez, A., Gupta, A., Ramirez, M.G., Liu, P.S., Kayagaki, N., Ciferri, C., Dixit, V.M., and Dueber, E.C. (2016). GsdmD p30 elicited by caspase-11 during pyroptosis forms pores in membranes. Proc. Natl. Acad. Sci. USA *113*, 7858–7863. https://doi.org/10.1073/pnas.1607769113.
20. Orning, P., Weng, D., Starheim, K., Ratner, D., Best, Z., Lee, B., Brooks, A., Xia, S., Wu, H., Kelliher, M.A., et al. (2018). Pathogen blockade of TAK1 triggers caspase-8-dependent cleavage of gasdermin D and cell death. Science *362*, 1064–1069. https://doi.org/10.1126/science.aau2818.
21. Hsu, H.-Y., and Wen, M.-H. (2002). Lipopolysaccharide-mediated reactive oxygen species and signal transduction in the regulation of interleukin-1 gene expression. J. Biol. Chem. *277*, 22131–22139. https://doi.org/10.1074/jbc.M111883200.
22. Hei, T.K., Liu, S.X., and Waldren, C. (1998). Mutagenicity of arsenic in mammalian cells: role of reactive oxygen species. Proc. Natl. Acad. Sci. USA *95*, 8103–8107. https://doi.org/10.1073/pnas.95.14.8103.
23. Underhill, D.M., Rossnagle, E., Lowell, C.A., and Simmons, R.M. (2005). Dectin-1 activates Syk tyrosine kinase in a dynamic subset of macrophages for reactive oxygen production. Blood *106*, 2543–2550. https://doi.org/10.1182/blood-2005-03-1239.
24. Haggie, P.M., and Verkman, A.S. (2008). Monomeric CFTR in plasma membranes in live cells revealed by single molecule fluorescence imaging. J. Biol. Chem. *283*, 23510–23513. https://doi.org/10.1074/jbc.C800100200.
25. Xiao, H., Jedrychowski, M.P., Schweppe, D.K., Huttlin, E.L., Yu, Q., Heppner, D.E., Li, J., Long, J., Mills, E.L., Szpyt, J., et al. (2020). A quantitative tissue-specific landscape of protein redox regulation during aging. Cell *180*, 968–983.e24. https://doi.org/10.1016/j.cell.2020.02.012.
26. Saurin, A.T., Neubert, H., Brennan, J.P., and Eaton, P. (2004). Widespread sulfenic acid formation in tissues in response to hydrogen peroxide. Proc. Natl. Acad. Sci. USA *101*, 17982–17987. https://doi.org/10.1073/pnas.0404762101.
27. von Moltke, J., Trinidad, N.J., Moayeri, M., Kintzer, A.F., Wang, S.B., van Rooijen, N., Brown, C.R., Krantz, B.A., Leppla, S.H., Gronert, K., and Vance, R.E. (2012). Rapid induction of inflammatory lipid mediators by the inflammasome in vivo. Nature *490*, 107–111. https://doi.org/10.1038/nature11351.
28. Rathkey, J.K., Zhao, J., Liu, Z., Chen, Y., Yang, J., Kondolf, H.C., Benson, B.L., Chirieleison, S.M., Huang, A.Y., Dubyak, G.R., et al. (2018). Chemical disruption of the pyroptotic pore-forming protein gasdermin D inhibits inflammatory cell death and sepsis. Sci. Immunol. *3*, eaat2738. https://doi.org/10.1126/sciimmunol.aat2738.
29. Humphries, F., Shmuel-Galia, L., Ketelut-Carneiro, N., Li, S., Wang, B., Nemmara, V.V., Wilson, R., Jiang, Z., Khalighinejad, F., Muneeruddin, K., et al. (2020). Succination inactivates gasdermin D and blocks pyroptosis. Science *369*, 1633–1637. https://doi.org/10.1126/science.abb9818.
30. Hu, J.J., Liu, X., Xia, S., Zhang, Z., Zhang, Y., Zhao, J., Ruan, J., Luo, X., Lou, X., Bai, Y., et al. (2020). FDA-approved disulfiram inhibits pyroptosis by blocking gasdermin D pore formation. Nat. Immunol. *21*, 736–745. https://doi.org/10.1038/s41590-020-0669-6.
31. Li, S., Wang, L., Xu, Z., Huang, Y., Xue, R., Yue, T., Xu, L., Gong, F., Bai, S., Wu, Q., et al. (2021). ASC deglutathionylation is a checkpoint for NLRP3 inflammasome activation. J. Exp. Med. *218*, e20202637. https://doi.org/10.1084/jem.20202637.
32. Wang, Y., Shi, P., Chen, Q., Huang, Z., Zou, D., Zhang, J., Gao, X., and Lin, Z. (2019). Mitochondrial ROS promote macrophage pyroptosis by inducing GSDMD oxidation. J. Mol. Cell Biol. *11*, 1069–1082. https://doi.org/10.1093/jmcb/mjz020.
33. Meissner, F., Molawi, K., and Zychlinsky, A. (2008). Superoxide dismutase 1 regulates caspase-1 and endotoxic shock. Nat. Immunol. *9*, 866–872. https://doi.org/10.1038/ni.1633.
34. Xia, S., Zhang, Z., Magupalli, V.G., Pablo, J.L., Dong, Y., Vora, S.M., Wang, L., Fu, T.-M., Jacobson, M.P., Greka, A., et al. (2021). Gasdermin D pore structure reveals preferential release of mature interleukin-1. Nature *593*, 607–611. https://doi.org/10.1038/s41586-021-03478-3.

35. Bambouskova, M., Potuckova, L., Paulenda, T., Kerndl, M., Mogilenko, D.A., Lizotte, K., Swain, A., Hayes, S., Sheldon, R.D., Kim, H., et al. (2021). Itaconate confers tolerance to late NLRP3 inflammasome activation. Cell Rep. *34*, 108756. https://doi.org/10.1016/j.celrep.2021.108756.

36. Tsujimoto, K., Jo, T., Nagira, D., Konaka, H., Park, J.H., Yoshimura, S.I., Ninomiya, A., Sugihara, F., Hirayama, T., Itotagawa, E., et al. (2023). The lysosomal Ragulator complex activates NLRP3 inflammasome in vivo via HDAC6. EMBO J. *42*, e111389. https://doi.org/10.15252/embj.2022111389.

37. Eng, J.K., Jahan, T.A., and Hoopmann, M.R. (2013). Comet: an open-source MS/MS sequence database search tool. Proteomics *13*, 22–24. https://doi.org/10.1002/pmic.201200439.

38. Huttlin, E.L., Jedrychowski, M.P., Elias, J.E., Goswami, T., Rad, R., Beausoleil, S.A., Villén, J., Haas, W., Sowa, M.E., and Gygi, S.P. (2010). A tissue-specific atlas of mouse protein phosphorylation and expression. Cell *143*, 1174–1189. https://doi.org/10.1016/j.cell.2010.12.001.

39. Schweppe, D.K., Prasad, S., Belford, M.W., Navarrete-Perea, J., Bailey, D.J., Huguet, R., Jedrychowski, M.P., Rad, R., McAlister, G., Abbatiello, S.E., et al. (2019). Characterization and optimization of multiplexed quantitative analyses using high-field asymmetric-waveform ion mobility mass spectrometry. Anal. Chem. *91*, 4010–4016. https://doi.org/10.1021/acs.analchem.8b05399.

40. McAlister, G.C., Nusinow, D.P., Jedrychowski, M.P., Wühr, M., Huttlin, E.L., Erickson, B.K., Rad, R., Haas, W., and Gygi, S.P. (2014). MultiNotch MS3 enables accurate, sensitive, and multiplexed detection of differential expression across cancer cell line proteomes. Anal. Chem. *86*, 7150–7158. https://doi.org/10.1021/ac502040v.

41. Beausoleil, S.A., Villén, J., Gerber, S.A., Rush, J., and Gygi, S.P. (2006). A probability-based approach for high-throughput protein phosphorylation analysis and site localization. Nat. Biotechnol. *24*, 1285–1292. https://doi.org/10.1038/nbt1240.

STAR★METHODS

KEY RESOURCES TABLE

REAGENT or RESOURCE	SOURCE	IDENTIFIER
Antibodies		
Mouse monoclonal Anti-β actin	MilliporeSigma	A5441; RRID:AB_476744
Mouse monoclonal Anti-β-Actin	Cell Signaling Technology	3700S; RRID:AB_2242334
Peroxidase AffiniPure Goat Anti-Mouse IgG (H + L)	Jackson ImmunoResearch	115-035-003; RRID:AB_10015289
Peroxidase AffiniPure Goat Anti-Rabbit IgG (H + L)	Jackson ImmunoResearch	111-035-003; RRID:AB_2313567
Rabbit monoclonal Anti-GSDMD	Abcam	ab209845; RRID:AB_2783550
Rabbit monoclonal Anti-RagA	Cell Signaling Technology	4357S; RRID:AB_10545136
Rabbit polyclonal Anti-tagRFP	Evrogen	AB233; RRID:AB_2571743
Rabbit monoclonal Anti-caspase-8	Cell Signaling Technology	4790S; RRID:AB_10545768
Rabbit monoclonal Anti-RIPK1	Cell Signaling Technology	3493S; RRID:AB_2305314
Bacterial and virus strains		
Escherichia coli TOP10	Invitrogen	C404010
Competent *Escherichia coli* DH5α	Jonathan Kagan Laboratory	N/A
Chemicals, peptides, and recombinant proteins		
Lethal factor flagellin fusion protein (Lfn-Fla)	Jonathan Kagan Laboratory[17]	N/A
Protective antigen	List Biological Labs	#171E
BamHI restriction enzyme	Thermo	ER0055
Benzonase	EMD Millipore	70664–3
β-glucan peptide	Invivogen	tlrl-bgp
Blasticidin	Fisher Scientific	A1113903
Bond-Breaker TCEP solution, neutral pH	ThermoFisher Scientific	77720
CM-H_2DCFDA	ThermoFisher Scientific	C6827
Complete protease inhibitor tablets	Sigma Aldrich	11836170001
Dimethyl sulfoxide	Sigma Aldrich	D2438
Doxycycline hyclate	Sigma Aldrich	D9891-1G
dNTP mix	Quanta Biosciences	95062–200
Dulbecco's MEM, high glucose, L-glut, pyruvate	ThermoFisher Scientific	11995–073
E. coli LPS Serotype O111:B4 S-form	Enzo Life Sciences	ALX-581-012-L002
Ultrapure LPS, E. coli 0111:B4	Invivogen	tlrl-3pelps
EcoRI restriction enzyme	Thermo	ER0275
EDTA (sterile 0.5 M solution)	Fisher Scientific	15575–020
Murine recombinant LPS binding protein (LBP)	R&D Systems	6635-LP/CF
Fetal bovine serum	ThermoFisher Scientific/GIBCO	10500064
G418	Invivogen	ant-gn-5
G418	SIGMA (Roche)	4727894001
Glycerol	Fisher	BP229-1
1 M HEPES solution, pH 7.0	ThermoFisher Scientific	11995–073
Hydrogen peroxide (30% w/w) stock solution	MilliporeSigma	H1009-100ML
L-glutamine	ThermoFisher Scientific	25030081; 25030164
Lipofectamine 2000	Invitrogen	11668019
Neutravidine agarose	ThermoFisher Scientific	29200
Nonidet P40 (NP-40)	United States Biochemical	19628
NotI-HF restriction enzyme	NEB	#R3189

(*Continued on next page*)

Continued

REAGENT or RESOURCE	SOURCE	IDENTIFIER
OptiMEM reduced serum media	ThermoFisher Scientific	31985062
Pen/Strep	ThermoFisher Scientific	15-140-122; 15-140-163
Phosphate-buffered saline (PBS); pH 7.4	ThermoFisher Scientific/GIBCO	10010–023
Phusion HF Polymerase	ThermoFisher Scientific	F-530L
Polybrene	MerckMillipore	TR-1003-G
Puromycin	Invivogen	ant-pr-1
Propidium iodide	MilliporeSigma	P4864-10ML
Rotenone	Tocris	3616
SalI-HF restriction enzyme	NEB	#R3138
Sepharose 6B beads	MilliporeSigma	CL6B200-100ML
Sodium Chloride	MilliporeSigma	S9625
Sodium m-Arsenite	MilliporeSigma	S7400-100G
Sodium Pyruvate	ThermoFisher Scientific	11360070
SDS solution 20%	ThermoFisher Scientific	AM9820
Tris base	MilliporeSigma	T-1503
TTFA (2-Thenoyltrifluoroacetone)	Sigma	T27006-25G
T4 ligase	NEB	M0202S
N-ethylmaleimide	MilliporeSigma	04259
Biotin-maleimide	Vector Laboratories	SP-1501-12
Iodoacetamide	Sigma-Aldrich	Cat#I1149
Lys-C	Wako Chemicals	Cat#125–05061
Trypsin	Promega	Cat#V5113
Hydroxylamine	MilliporeSigma	Cat#438227
Neocuprine	MilliporeSigma	N1501
DTPA	MilliporeSigma	D6518
EPPS	MilliporeSigma	Cat#E9502
Cysteine-reactive phosphate tags (CPTs)	Chouchani lab[25]	N/A
Methanol	VWR	BDH1135-4LG
Urea	MilliporeSigma	U5378
Disulfiram	MilliporeSigma	86720
Critical commercial assays		
100 mL Tip Neon Transfection Kit	ThermoFisher Scientific	MPK10096
CyQuant LDH Cytotoxicity Assay Kit	ThermoFisher Scientific	C20301
Pierce BCA Protein Assay kit	ThermoFisher Scientific	23227
Micro BCA™ Protein Assay Kit	ThermoFisher Scientific	Cat#23235
Sep-Pak C18 Cartridges	Waters	Cat#WAT054955
16-plex TMT reagents	ThermoFisher Scientific	Cat#A44520
Q5 Site-directed mutagenesis kit	NEB	E0554S
BFP catcher beads	Antibodies online	ABIN5311512
Experimental models: Cell lines		
Cas9 KI iBMDM	Jonathan Kagan Laboratory[17]	N/A
iBMDM Cas9 KI Tet3G Doxycycline Inducible NT-GSDMD-BFP	Jonathan Kagan Laboratory[17]	N/A
iBMDM Cas9 KI Tet3G Doxycycline Inducible NT-GSDMD-BFP pXPR-054-empty vector	Jonathan Kagan Laboratory[17]	N/A
iBMDM Cas9 KI Tet3G Doxycycline Inducible NT-GSDMD-BFP pXPR-054-RagC-sgRNA1	Jonathan Kagan Laboratory[17]	N/A

(*Continued on next page*)

Continued

REAGENT or RESOURCE	SOURCE	IDENTIFIER
iBMDM Cas9 KI Tet3G Doxycycline Inducible NT-GSDMD-BFP pXPR-054-RagA-sgRNA1	Jonathan Kagan Laboratory[17]	N/A
iBMDM Cas9 KI Tet3G Doxycycline Inducible NT-GSDMD-BFP + Non-target synthetic sgRNA	This paper	N/A
iBMDM Cas9 KI Tet3G Doxycycline Inducible NT-GSDMD-BFP + RagA synthetic sgRNA-1	This paper	N/A
iBMDM Cas9 KI Tet3G Doxycycline Inducible NT-GSDMD-BFP + RagA synthetic sgRNA-2	This paper	N/A
iBMDM Cas9 KI Tet3G Doxycycline Inducible NT-GSDMD-BFP + RagA synthetic sgRNA-3	This paper	N/A
iBMDM Cas9 KI Tet3G Doxycycline Inducible NT-GSDMD-BFP + RIPK1 synthetic sgRNA-1	This paper	N/A
iBMDM Cas9 KI Tet3G Doxycycline Inducible NT-GSDMD-BFP + RIPK1 synthetic sgRNA-2	This paper	N/A
iBMDM Cas9 KI Tet3G Doxycycline Inducible NT-GSDMD-BFP + Caspase-8 synthetic sgRNA-1	This paper	N/A
iBMDM Cas9 KI Tet3G Doxycycline Inducible NT-GSDMD-BFP + Caspase-8 synthetic sgRNA-2	This paper	N/A
GSDMD KO iBMDM	Jonathan Kagan Laboratory[17]	N/A
GSDMD KO iBMDM Tet3G	This paper	N/A
GSDMD KO iBMDM Tet3G pRETROX-TRE3G empty vector	This paper	N/A
GSDMD KO iBMDM Tet3G Doxycycline Inducible NT-GSDMD	This paper	N/A
GSDMD KO iBMDM Tet3G Doxycycline Inducible NT-GSDMD-C192A	This paper	N/A
GSDMD KO iBMDM Tet3G Doxycycline Inducible NT-GSDMD-No Cys (C39A, C57A, C77A, C122A, C192A, C265A)	This paper	N/A
GSDMD KO iBMDM Tet3G Doxycycline Inducible NT-GSDMD-I105N	This paper	N/A
GSDMD KO iBMDM Tet3G Doxycycline Inducible NT-GSDMD-I105N-C39A	This paper	N/A
GSDMD KO iBMDM Tet3G Doxycycline Inducible NT-GSDMD-I105N-C192A	This paper	N/A
GSDMD KO iBMDM Tet3G Doxycycline Inducible NT-GSDMD-I105N-No Cys (C39A, C57A, C77A, C122A, C192A, C265A)	This paper	N/A
GSDMD KO iBMDM Tet3G Doxycycline Inducible NT-GSDMD-I105N C192only (C39A, C57A, C77A, C122A, C265A)	This paper	N/A
GSDMD KO iBMDM pMSCV IRES EGFP empty vector	This paper	N/A
GSDMD KO iBMDM Full-length GSDMD	This paper	N/A
GSDMD KO iBMDM Full-length GSDMD-C39A	This paper	N/A
GSDMD KO iBMDM Full-length GSDMD-C192A	This paper	N/A
GSDMD KO iBMDM Full-length GSDMD-No Cys (C39A, C57A, C77A, C122A, C192A, C265A)	This paper	N/A
Platinum-GP retroviral packaging cell line	Cell Biolabs	RV-103

(*Continued on next page*)

Continued

REAGENT or RESOURCE	SOURCE	IDENTIFIER
Oligonucleotides		
Q5 mutagenesis_mGSDMD_C192A_fwd: TGGAGCTTTAgccTTGAAGGGTGAAGGCAAG	IDT	N/A
Q5 mutagenesis_mGSDMD_C192A_rev: GGCAGCGTAAACTGGCCT	IDT	N/A
mGSDMD_C39A_fwd: CAGGCCCTACgccCTTCTGAACAGGAAATTTTC	IDT	N/A
mGSDMD_C39A_rev: AAGCTGGTGGAGTTCCGC	IDT	N/A
NotI_Kozak_mGSDMD_fwd: ttctctttGCGGCCGCGCCACCATGCCATCGGCC	IDT	N/A
SalI_Myc-tag_mGSDMD_rev tttctctttGTCGACcta CAGATCCTCTTCTGAGATGAGT TTTTGTTCACAAGGTTTCTGGCCTAGACTTGac	IDT	N/A
mGSDMD_I105N-fwd: GGAGAAGGGAAAAATTCTGGTGGGGCT	Evavold et al.[17]	N/A
mGSDMD_I105N-rev: AGCCCCACCAGAATTTTTCCCTTCTCC	Evavold et al.[17]	N/A
mGSDMD_C39A-fwd: CTTCAGGCCCTACGCCCTTCTGAACAGG	This paper, Merck	N/A
mGSDMD_C39A-rev: CCTGTTCAGAAGGGCGTAGGGCCTGAAG	This paper, Merck	N/A
mGSDMD_C192A-fwd: CCTGGAGCTTTAGCCTTGAAGGGTGAAG	This paper, Merck	N/A
mGSDMD_C192A-rev: CTTCACCCTTCAAGGCTAAAGCTCCAGG	This paper, Merck	N/A
mGSDMD_A192C-fwd: CCTGGAGCTTTATGCTTGAAGGGTGAAG	This paper, Merck	N/A
mGSDMD_A192C-rev: CTTCACCCTTCAAGCATAAAGCTCCAGG	This paper, Merck	N/A
BamHI-GSDMD-fwd: CGGATCCGCCACCATGCCATCGGCCTTTGAGAAAG	Evavold et al.[17]	N/A
GSDMD-NT-rev: GGAATTCCCTAATCTGACAGGA GACTGAGCTGC	This paper, Merck	N/A
Non-target complete synthetic sgRNA: AAAUGUGAGAUCAGAGUAAU	IDT	N/A
RagA complete synthetic sgRNA-1: GGTTCCCCAAGAATCGGACG	IDT	Mm.Cas9.RRAGA.1.AP
RagA complete synthetic sgRNA-2: GATCAGCTGATAGACGATGC	IDT; Evavold et al.[17]	N/A
RagA complete synthetic sgRNA-3: GTGGGAGTGCTCCACGTCGA	IDT	Mm.Cas9.RRAGA.1.AA
RIPK1 complete synthetic sgRNA-1: TACACGTCCGACTTCTCCGT	IDT	Mm.Cas9.RIPK1.1.AA
RIPK1 complete synthetic sgRNA-2: AGTCGAGTGGTGAAGCTACT	IDT	Mm.Cas9.RIPK1.1.AC
Caspase-8 complete synthetic sgRNA-1: CTTCCTAGACTGCAACCGAG	IDT	Mm.Cas9.CASP8.1.AA
Caspase-8 complete synthetic sgRNA-2: GTGGGATGTAGTCCAAGCAC	IDT	Mm.Cas9.CASP8.1.AB
Recombinant DNA		
pRetroX-Tet3G	Clontech	631188
pRETROX-TRE3G	Clontech	631188

(*Continued on next page*)

Continued

REAGENT or RESOURCE	SOURCE	IDENTIFIER
pRETROX-TRE3G_NT-GSDMD	This paper	N/A
pRETROX-TRE3G_NT-GSDMD-I105N	This paper	N/A
pRETROX-TRE3G_NT-GSDMD-I105N-C192only	This paper	N/A
pRETROX-TRE3G_NT-GSDMD-I105N-C192A	This paper	N/A
pRETROX-TRE3G_NT-GSDMD-I105N-C39A	This paper	N/A
pRETROX-TRE3G_NT-GSDMD-I105N-No Cys	This paper	N/A
pRETROX-TRE3G_NT-GSDMD-C192A	This paper	N/A
pRETROX-TRE3G_NT-GSDMD-No Cys	This paper	N/A
pMSCV IRES EGFP-GSDMD-Myc	This paper	N/A
pMSCV IRES EGFP-GSDMD-C39A-Myc	This paper	N/A
pMSCV IRES EGFP-GSDMD-C192A-Myc	This paper	N/A
pMSCV IRES EGFP-GSDMD-No Cys-Myc	This paper	N/A
Software and algorithms		
SparkControl v.3.2	Tecan	N/A
ImageJ	NIH	https://imagej.nih.gov/ij/
Xcalibur	ThermoFisher Scientific	Cat#OPTON-30965
Comet	Eng et al.[37]	http://comet-ms.sourceforge.net
Masspike (in house)	Huttlin et al.[38]	N/A
Protein Digestion Simulator	Pacific Northwest National Laboratory	https://pnnl-comp-mass-spec.github.io/Protein-Digestion-Simulator/
R version 4.0.2	R Project	https://www.r-project.org
RStudio 2022.02.3 + 492	R Studio Team	https://rstudio.com
Prism 6 and 8.0	GraphPad	https://www.graphpad.com/scientific-software/prism/
FlowJo (v10.3.0)	FlowJo	https://www.flowjo.com/
Microsoft Excel	Microsoft	N/A
Illustrator CC 2019	Adobe	https://www.adobe.com/products/illustrator.html
Zen Black	Zeiss	https://www.micro-shop.zeiss.com/en/us/softwarefinder/software-categories/zen-black/
Other		
Live cell imaging, μ-Dish 35 mm, high	Ibidi	81156
μ-slide 8 well	Ibidi	80826
LSM880 confocal laser scanning microscope with Airy scan	Zeiss	N/A
Spark microplate reader	Tecan	N/A
FACSMelody Cell Sorter	BD	N/A
BD LSRFortessa Cell Analyzer	BD	N/A
Costar, Black 96 well plate w/ lid, clear flat bottom, TC treated	Costar	3603
NuPAGE 4–12% gradient gels	ThermoFisher	NP0321BOX; NP0323BOX
MOPS SDS Running buffer (20x)	ThermoFisher	NP0001
Incucyte SX5	Sartorius	N/A
Synergy Mx microplate reader	Biotek	1897
ChemiDoc MP Imaging System	BioRad	17001402
Zeba Desalt Spin columns (7kDa cutoff)	ThermoFisher Scientific	89891
Orbitrap Eclipse Mass Spectrometer	ThermoFisher Scientific	Cat#FSN04-10000
EASY-nLC 1200 System	ThermoFisher Scientific	Cat#LC140
FAIMSPro	ThermoFisher Scientific	Cat#FMS02-10001

RESOURCE AVAILABILITY

Lead contact

Further information and requests for resources and reagents should be directed to and will be fulfilled by the lead contact, Jonathan C. Kagan (jonathan.kagan@childrens.harvard.edu).

Materials availability

All materials generated in this study are available from the lead contact.

Data and code availability

- All data reported in this paper will be shared by the lead contact upon request.
- This paper does not report original code.
- Any additional information required to reanalyze the data reported in this paper is available from the lead contact upon request.

EXPERIMENTAL MODEL AND SUBJECT DETAILS

Cell culture

All cells were cultured in humidified incubators at 37°C and 5% CO_2. Immortalized bone marrow-derived macrophages (iBMDMs) and Platinum GP cells (Cell Biolabs) were cultured in DMEM supplemented with 10% fetal bovine serum (FBS), Penicillin + Streptomycin, L-Glutamine and Sodium pyruvate, herafter referred to as complete DMEM (cDMEM) and cultured in tissue-culture treated 10 cm dishes or T175 tissue culture flasks (Corning). iBMDMs and Platinum-GP cells were passaged using PBS + 4 mM EDTA or 0.25% trypsin + EDTA (Gibco), respectively.

METHOD DETAILS

Reagents and antibodies

E. coli LPS (serotype O:111 B4) was purchased from Enzo Biosciences as a ready-to-use stock solution of 1 mg/mL β-glucan-peptide was from Invivogen and dissolved at 5 mg/mL in sterile PBS. zVAD-FMK (Invivogen) was resuspended in sterile DMSO to a concentration of 20 mM and used at a final concentration of 20 μM or 50 μM. Propidium iodide solution (1 mg/mL) was purchased from MilliporeSigma or Thermo Scientific. RIPK1 inhibitor (7-Cl-O-Nec-1) and RIPK3 inhibitor (GSK'872) were both from MilliporeSigma. TAK1 inhibitor (5z7) was purchased from Sigma and resuspended in sterile DMSO at 2.5 mM. Disulfiram (Sigma-Aldrich) was prepared in sterile DMSO (50 mM). Doxycycline hyclate was from Sigma and resupended at 1 mM or 1 mg/mL in sterile H_2O. Sodium arsenite (MilliporeSigma) was dissolved in H_2O to a concentration of 100 mM and sterile-filtered through a 0.2 μm syringe filter before use. Rotenone (Sigma-Aldrich) was disolved in sterile DMSO at 12.7 mM. Recombinant murine LBP was purchased from R&D, diluted to 1 mg/mL in sterile PBS and snap-frozen in LN2. G418 was from Invivogen and puromycin was from Gibco. Stabilized hydrogen perodxide (H_2O_2) solution (30%) was purchased from Sigma-Aldrich.

Following antibodies were used as primary antibodies for immunoblotting: mouse monoclonal anti-β-actin (MilliporeSigma, 1:5000), rabbit monoclonal anti-GSDMD (Abcam, 1:1000), rabbit monoclonal anti-RagA (Cell Signaling, 1:1000), rabbit monoclonal anti-caspase-8 (Cell Signaling, 1:1000), rabbit monoclonal anti-RIPK1 (Cell signaling, 1:1000), rabbit polyclonal anti-tagRFP (Evrogen, 1:1000). HRP-conjugated goat anti-mouse and goat anti-rabbit IgG (H + L) secondary antibodies were from Jackson ImmunoResearch and diluted 1:5000.

Constructs

Gene encoding mouse full-length GSDMD was ordered from Synobiological. gBlock encoding full-length mouse GSDMD with all cysteines in the N-terminal domain mutated to alanine and C-terminal Myc-tag (No Cys mutant) was ordered from Integrated DNA Technologies. WT and No Cys mutant full-length GSDMD constructs were cloned into pMSCV IRES EGFP using *NotI* and *SalI* restriction sites. In order to add a C-terminal Myc-tag to WT GSDMD, sequence encoding the tag was included in the reverse primer. Point mutations (C39A and C192A) were introduced using the Q5 mutagenesis kit (NEB) according to manufacturer's protocols.

N-terminal GSDMD (1–276; WT and No Cys mutant) was amplified by PCR and subcloned into pRETROX-TRE3G vector using BamHI and EcoRI restriction sites. I105N, C39A, C192A or A192C point mutations in were introduced by site-directed mutagenesis. All constructs were verified by Sanger sequencing.

Cell lines

iBMDMs derived from a Cas9 knock-in mouse or a GSDMD KO mouse and Cas9-expressing iBMDMs expressing an NT-GSDMD-tagBFP fusion protein with an I105N mutation (referred to as NT-GSDMD) under the control of a Dox-inducible promoter (parental line used to generate KOs for Figure 1; empty vector-transduced and RagA KO cells used in Figures 2, 3, and 4) were generated previously.[17]

Dox-inducible murine NT-GSDMD variants (with or without I105N mutation) were introduced into GSDMD KO iBMDMs by sequential transduction with two pantropic retroviruses. First, the TET3G tetracycline transactivator protein was introduced. To do so, 1.2 × 10^6 Platinum-GP retrovirus packaging cells were seeded per well in a 6-well tissue culture plate. On the next day, cells were transfected with pCMV-VSV-G (1.5 μg) and pRETROX TET3G (2.5 μg) (Clontech) using Lipofectamine 2000 (10 μL). The same day 3 × 10^5 GSDMD KO cells were seeded per well of 6-well plate. The next day, medium was replaced with 1 mL of complete medium with polybrene (2 μg/mL) and retroviral supernatant was filtered through 0.45-micron syringe filter and added to cells. Three days after transduction, transduced cells were selected by growth in cDMEM including 1.5 mg/ml G-418. Clonal cell lines were derived by limited serial dilution. GSDMD-NT(I105N) variants were introduced into single cell GSDMD-KO/Tet3G cell line by transduction of respective pantropic viruses using the protocol described above where pRETROX TRE3G vectors encoding GSDMD-NT(I105N) variants were used as transfer plasmids. Selection of transduced cells was performed by growth in 10 μg/mL puromycin and 1.5 mg/ml G-418 medium.

To stably introduce full-length murine GSDMD variants into cells, 2.5 × 10^6 HEK293T cells were seeded in a 10 cm cell culture dish. On the next day, cells were transfected with 9 μg of pMSCV IRES EGFP encoding the protein of interest, 6 μg of pCL-ECO and 3 μg of pCMV-VSVG using Lipofectamine 2000 (ThermoFisher) according to the manufacturer's instructions. After 18–24 h at 37°C, medium was changed to 6 mL of cDMEM and virus was collected 24 h afterward. Supernatants were centrifuged to pellet cellular debris (400 x g, 5 min) and filtered through a 0.45 μm PVDF syringe filter. ~1 × 10^6 GSDMD KO iBMDMs were transduced twice on two consecutive days in a 6-well plate by adding 4.5 mL of viral supernatant supplemented with Polybrene (1:2000; EMD Millipore) per well, followed by centrifugation for 1 h at 1250 x g and 30°C. GFP^+ cells were sorted twice on a FACSMelody cell sorter (BD Biosciences). Since GFP expression in these cells correlates with transgene expression, sorting on select bins during the second sort allowed for the control of transgene expression level. This approach was used to produce cell lines with near-endogenous and low expression of GSDMD. Transgene expression was confirmed by immunobloting.

Generation of KO cell lines using CRISPR/Cas9 technology

CRISPR KO cell lines were generated by electroporation of synthetic sgRNAs into Cas9-expressing iBMDMs using the Neon transfection system (Thermo Fisher) as described before.[17] Briefly, 1.2 × 10^6 Cas9-expressing iBMDMs were resuspended in 120 μL of R buffer, mixed with 2 μL of sgRNA (ordered from IDT and resuspended in nuclease-free water at a concentration of 100 μM) and electroporated using a 100 μL electroporation pipette tip with two 10 ms pulses at a voltage of 1400 V. Cells were then dispensed directly into a 6-well plate containing 3 mL of cDMEM and cultured for 3–5 days before assessing bulk KO efficiency by immunoblot. These cell lines were further single cell cloned by limited serial dilution to obtain clonal KO cell populations with complete ablation of the target protein. sgRNA sequences were previously published or pre-designed by IDT.

GSDMD cleavage and oligomerization assay

0.5 × 10^6 iBMDMs expressing NT-GSDMD under a Dox-inducible promoter were seeded in 12-well plates in 1 mL of cDMEM and incubated at 37°C and 5% CO_2 overnight. Media was exchanged for 1 mL of Opti-MEM containing 2 μg/mL of Dox to induce the expression of NT-GSDMD-tagBFP for 8 h at 37°C and 5% CO_2. As indicated, cells were cotreated with ROS-inducing agents or PAMPs. 50 μL of Opti-MEM containing rotenone (5 μM final concentration), TTFA (100 μM final concentration) or sodium arsenite (20 μM final concentration) was added to the cell culture media after 4 h. LPS (1 μg/mL) and β-glucan peptide (1 mg/mL) were present in the cell culture media throughout the entire 8 h incubation period. To ensure efficient priming by LPS in the absence of serum, 2 μg/mL of recombinant murine LBP was added to LPS stimulated cells. To end the reaction 250 μL of 5X SDS loading buffer was added to each well to capture proteins present in both the cell lysates and supernatants. Samples were homogenized by passing them through a 26-gauge needle, split equally into two tubes and 75 μL of TCEP or H_2O was added to generate non-reducing and reducing immunoblot samples. After heating to 65°C for 10 min, proteins were separated by SDS-PAGE on a 4%–12% acrylamide gradient gel (Thermo Fisher) and transgene was detected via immunoblot using a tag-RFP-specific antibody. Since the GSDMD pore is resistant to SDS under non-reducing conditions, oligomerization of NT-GSDMD was indicated by a gel shift toward higher molecular weight. Densitometry analyses to quantify band intensities were performed using ImageJ software. To quantify GSDMD processing, intensity of band representing NT-GSDMD was quantified and normalized to corresponding actin signal. Band intensities in RagA-deficient cells were then normalized to signal in WT cells (separate for each experiment). To quantify GSDMD oligomerization, raw band intensity of oligomer band was divided by band intensity of monomer band in the same lane.

Dox-induction of NT-GSDMD

0.5–1 × 10^5 iBMDMs expressing NT-GSDMD under a Dox-inducible promoter (WT cells transduced with empty vector or electroporated with non-target sgRNA, RagA KO, caspase-8 KO or RIPK1 KO) were seeded in duplicate or triplicate wells in a black 96-well plate in 200 μL of cDMEM. To induce the transgene, media was exchanged for 200 μL fresh cDMEM containing Dox (0.5–2 μg/ml as indicated in Figure legends) and plasma membrane perforation/cell lysis were quantified by PI staining and LDH assay after 8 h or 16 h as described below. For inhibitor studies, cells were pretreated with zVAD (20 μM or 50 μM), RIPK1 inhibitor (1 μM or 5 μM), or RIPK3 inhibitor (1 μM or 5 μM) for 1 h and inhibitors were co-administered during Dox treatment. Disulfiram (25 μM) was added after 4 h of Dox treatment. To induce ROS, cells were co-treated with ROS-inducing agents or PAMPs. 10 μL of cDMEM containing rotenone (5 μM final concentration), TTFA (100 μM final concentration) or sodium arsenite (20 μM final

concentration) was added to the cell culture media after 4 h. LPS and β-glucan peptide were present in the cell culture media during the entire stimulation. For direct ROS stimulation, 10 μL of stabilized hydrogen peroxide was added to the cells after 6 h to a final concentration of 625 μM.

To assess fraction of cells expressing NT-GSDMD-BFP, cells were detached using 150 μL of PBS + 4 mM EDTA and analyzed via flow cytometry on a BD LSRFortessa Cell Analyzer (BD Biosciences). Transgene expression was detected in the PacBlue channel.

Induction of caspase-8 and RIPK1-mediated pyroptosis by TAK1 inhibitor treatment

Co-treatment of cells with TAK1 inhibitor (5z7) and LPS was used to induce caspase-8- and RIPK1-dependent pyroptosis. 1×10^5 iBMDMs were seeded in duplicate wells in a black 96-well plate in 200 μL of cDMEM. After incubation at 37°C and 5% CO_2 for 1–2 h to facilitate cell attachment, media was exchanged for 200 μL fresh cDMEM containing 5z7 (250 nM) and LPS (1 μg/mL). Cells were incubated for another 3 or 6 h at 37°C and 5% CO_2 before quantifying cell death by PI staining and LDH release assay.

Propidium iodide staining and LDH assay

To assess plasma membrane perforation or cellular lysis as a proxy of cell death, we quantified fluorescence after PI staining or lactate dehydrogenase release using the CyQuant LDH cytotoxicity assay kit from Thermo Fisher. Briefly, 10 μL of pre-diluted PI solution was added to the cells (1:300 final dilution) 30 min prior to the end of the stimulation and following a centrifugation step to ensure all cells are in the bottom plane of the wells, (5 min at 400 x g) fluorescence was measured on a Tecan Spark or Biotek Synergy Mx device at an excitation wavelength of 530 nm and an emission wavelength of 617 nm. For the LDH assay, 50 μL of cell culture supernatant per well was transferred into a fresh 96-well plate before adding 50 μL of LDH assay buffer and incubation for 10–20 min at 37°C. Reaction was stopped by adding 50 μL of LDH stop solution to each well. Absorbance at 490 nm and 680 nm was meaured on a Tecan Spark or Biotek Synergy Mx plate reader. In both assays, signal was normalized to lysis control wells (equal number of cells lysed with detergent-containing lysis buffer).

To assess plasma membrane perforation in real-time we stained cells with PI as described above and determined fuorescence over time on a Tecan spark equilibrated to 37°C at atmospheric CO_2 (short term assays up to 2 h; media was supplemented with 50 mM HEPES, pH 7.0 to stabilize pH in culture media) or an Incucyte SX5 device (Sartorius) installed inside a tissue culture incubator at 37°C and 5% CO_2 (long term assays). PI fluorescence was detected in the orange channel of the Incucyte device at an integration time of 400 ms per image. Cells were segmented based on brightfield image and frequency of PI-positive cells was determined using commercial software provided with the Incucyte device.

Pulldown of oxidized GSDMD

Determination of relative cysteine oxidation was performed as described before with modifications.[26] 10×10^6 iBMDMs expressing NT-GSDMD under a Dox-inducible promoter (empty vector-transduced or RagA KO) were seeded in tissue culture-treated 10 cm dishes in 10 mL of cDMEM and incubated at 37°C and 5% CO_2 overnight. Media was exchanged for 10 mL of cDMEM containing 2 μg/mL of Dox to induce the expression of NT-GSDMD for 8 h at 37°C and 5% CO_2. As indicated, cells were co-treated with ROS-inducing agents. 500 μL of cDMEM containing rotenone (5 μM final concentration), TTFA (100 μM final concentration) or sodium arsenite (20 μM final concentration) was added to the cell culture media after 4 h. To study protein oxidation during NAIP/NLRC4-dependent pyroptosis, WT iBMDMs were stimulated with the synthetic toxin Flatox.[27] 10×10^6 WT iBMDMs were seeded in tissue culture-treated 10 cm dishes in 10 mL cDMEM and incubated at 37°C and 5% CO_2 overnight. Cells were primed by adding 10 mL of cDMEM containing 1 μg/mL of LPS and incubated at 37°C and 5% CO_2 for 4 h. Flatox was assembled by mixing 200 ng/mL of a Lethal-factor-Flagellin fusion protein (LFn-Fla; expressed and purified in insect cells as described previously[17]) and 500 ng/mL of anthrax protective antigen (List Biologicals) in cDMEM and added to cells (10 mL per plate) for 2 h.

Post-stimulation, cells were lifted using PBS + 4 mM EDTA, washed once in cold PBS, and directly resuspended with lysis buffer (RIPA) containing protease inhibitors and 100 mM N-ethylmaleimide to directly label cysteine-containing proteins at the time of lysis. After incubation on ice for 1 h, lysate was clarified by centrifugation at 16,000 x g at 4°C for 15 min. Protein concentrations were normalized by BCA Assay (Pierce ThermoFisher, Rockford, IL, USA) and excess N-ethylmaleimide was removed by filtration with Zeba spin columns with a 7 kDa cut-off (Thermo Fisher). Sulfenic acid residues were selectively reduced with 200 mM sodium arsenite and newly released free thiols were labeled by adding 1 mM biotin–maleimide. The mixture was incubated at 37°C for 1 h. Excess biotin–maleimide was removed using Zeba spin desalting columns. The protein mixture pre-cleared with Sepharose 6B beads (MilliporeSigma) on a rotator at room temperature for 2 h. The eluate was further incubated with NeutrAvidin agarose beads (Thermo Scientific) overnight 4°C to pull down biotin-labeled proteins. NeutrAvidin agarose was washed extensively with wash buffer (50 mM Tris, pH 7.5, 600 mM NaCl, 1 mM EDTA, 0.5% NP-40) and then cold PBS. Enriched proteins were eluted by boiling the NeutrAvidin agarose resin in 4x SDS buffer. Proteins were separated by SDS-PAGE and amount of oxidized NT-GSDMD was assessed by immunoblot using a tagBFP or GSDMD-specific antibody.

Fluorescence recovery after photo bleaching (FRAP)

FRAP experiments were performed on a Zeiss 880 laser scanning confocal microscope using the in-built FRAP module within the microscope control software Zen Black. 0.5×10^6 iBMDMs expressing BFP-tagged NT-GSDMD under the control of a Dox-inducible promoter were plated on a 35 mm μ-Dish (Ibidi; Munich, Germany) in 1 mL of cDMEM and incubated overnight at 37°C, 5% CO_2.

Media was exchanged for 1 mL of Opti-MEM containing 2 μg/mL Dox for 8 h to induce transgene expression. As indicated, cells were cotreated with ROS-inducing agents or PAMPs. 50 μL of Opti-MEM containing rotenone (5 μM final concentration), TTFA (100 μM final concentration) or sodium arsenite (20 μM final concentration) was added to the cell culture media after 4 h. Following treatments cells were scanned using a 63X oil immersion lens with the 405 nm laser. Regions of interest (ROI) were created at cell membranes and fluorescence bleached by rapid scanning of increased laser power (5–10%) to a bleach depth of 40–60%. Time-lapse images were acquired over a 3-min time course post-bleaching at 2-s intervals. Images were processed in Zen and FRAP data were fitted to a single exponential model using GraphPad Prism.

Data analysis was performed using previously published methods.[24] Fluorescence intensities of regions of interest (ROI) in the bleaching area (ROIb = bleached area) were recorded for each time point. The final data was normalized to pre-bleached intensities of the ROIs data and fitted to a single exponential recovery curve. Percent fluorescence recovery (mobile fraction) was calculated from the plateau (Vmax) of the fitted curves normalized to the total bleached fluorescence.

ROS measurements

0.5×10^6 iBMDMs expressing BFP-tagged NT-GSDMD under the control of a Dox-inducible promoter (RagA-deficient or WT cells) were plated on a 35 mm μ-Dish (Ibidi; Munich, Germany) in 1 mL of cDMEM and incubated overnight at 37°C, 5% CO_2. Media was exchanged for 1 mL of Opti-MEM containing 2 μg/mL Dox for 8 h to induce transgene expression. As indicated, cells were cotreated with ROS-inducing agents or PAMPs. 50 μL of Opti-MEM containing rotenone (5 μM final concentration), TTFA (100 μM final concentration) or sodium arsenite (20 μM final concentration) was added to the cell culture media after 4 h. LPS (1 μg/mL) and β-glucan peptide (1 mg/mL) were present in the cell culture media throughout the entire 8 h incubation period. To ensure efficient priming by LPS in the absence of serum, 2 μg/mL of recombinant murine LBP was added to LPS stimulated cells. Post-stimulation, cells were loaded with 5μM CM-H_2DCFDA (Thermofisher Scientific) for 10 min at 37°C. Cells were washed three times with PBS and immediately imaged at 37°C on a Zeiss 880 laser scanning confocal microscope using 63X oil immersion lens and 488 nm laser excitation. 5 × 5 tiled 2D images were obtained from at least three different areas per dish. Images were analyzed and mean fluorescence intensity (MFI) of segmented cells was measured using the intensity analysis function in ImageJ.

Proteomics

Strategy for determining the fraction of oxidized cysteine residues in GSDMD-NT was adapted from a previous publication.[25] iBMDMs expressing BFP-tagged NT-GSDMD under the control of a Dox-inducible promoter were seeded in ten 15 cm dishes (35×10^6 cells per dish) and grown overnight at 37°C, 5% CO_2. Expression of transgene was induced by adding 20 mL of cDMEM with 2 μg/mL Dox per plate followed by incubation for 8 h at 37°C, 5% CO_2. Cells and supernatants were collected and cells were pelleted by centrifugation at 500 x g, 10 min. Cell were resuspended in 20 mL of PBS, pH 7.4, split equally into two tubes and centrifuged again at 500 x g, 10 min. Cells pellets were lysed in 2.5 mL of labeling buffer (100 mM HEPES pH 8.5, 0.5% SDS, 4 M Urea, 1 mM EDTA, 1 mM DTPA, 10 μM neocuprine) supplemented with 90 units/mL benzonase, complete Mini protease inhibitors (Roche) and either 10 mM iodoacetamide or 10 mM cysteine-reactive phosphate tag (CPT) for differential labeling of unmodified cysteine residues.[25] Cell lysates were homogenized by passing them 10 times through an 18-gauge needle and sonication for 5 min (50% amplitude, 30s on/off cycles) and labeling reaction was allowed to proceed for 2 h at 37°C while gently rotating. Buffer was exchanged to IP buffer (25 mM HEPES pH 7.4, 150 mM NaCl, 1% NP-40, 0.1% SDS, 1 mM EDTA, 5% glycerol) and BFP-tagged GSDMD-NT was immunoprecipitated using 75 μL of BFP-catcher beads per sample using the fused BFP-domain as a handle. After incubation overnight at 4°C while gently rotating, beads were washed five times with 1 mL of IP buffer and bound proteins were eluted from the beads by adding 500 μL of labeling buffer supplemented with 5 mM TCEP and 10 mM iodoacetamide. After incubation for 2 h at 37°C while gently rotating (during this step reversibly modified/oxidized cysteines are reduced and labeled with iodoacetamide), beads were spun down (2000 x g, 1 min) and supernatants containing IAM and/or CPT labeled proteins were collected.

Proteins were then precipitated by adding tricholoroacetic acid to 20% v/v, and protein pellets were washed three times with cold methanol. Pellets were resuspended in 200 mM N-(2-Hydroxyethyl)piperazine-N′-(3-propanesulfonic acid) (EPPS) buffer pH = 8, and digested using a combination of Lys-C and trypsin at an enzyme-to-protein ratio of 1:100 overnight at 37°C. Each sample was labeled by 25 μg of the TMTpro-16 reagents for 1 h at room temperature. The reaction was quenched using 5 μL of 5% hydroxylamine for 15 min. Samples were then combined, dried, and reconstituted in 1% formic acid. The mixture was desalted via StageTip, dried in a speedvac, and reconstituted in a solution containing 5% acetonitrile and 4% formic acid for liquid chromatography-tandem mass spectrometry (LC-MS/MS).

All peptides were loaded onto an in-house 100-μm capillary column packed with 35 cm of Accucore 150 resin (2.6 μm,150 Å). The Orbitrap Eclipse Tribrid Mass Spectrometer (Thermo) coupled with an Easy-nLC 1200 (Thermo) was used for measurements. The sample was analyzed using a 180-min gradient consisting of 2%–23% acetonitrile, 0.125% formic acid at 500 nL/min flow rate. A FAIMSPro (Thermo) device was used to separate precursors[39] with default settings and three compensation voltages (−35V/-45V/-55V). Under each voltage, peptide ions were collected in data-dependent mode using a mass range of m/z 400–1600 using 2 s cycles. Resolution for MS1 was set at 120,000. Singly-charged ions were discarded. 35% normalized collisional energy (NCE) was used for for MS2. Dynamic exclusion window was set to 120 s for MS2 with maximum ion injection time of 50 ms. Quantification of TMT reporter ion were performed using the multinotch SPS-MS3 method with 45% NCE for MS3.[40]

All raw files were converted to mzXML,and searched with the Comet algorithm[37] on an in-house database search engine.[38] Database searching included all mouse (Mus musculus) entries from UniProt (http://www.uniprot.org, downloaded July 29th, 2020). Reversed sequences and common contaminants (keratins, trypsin, etc) were also appended to the list. The following parameters were used for searching: 25 ppm precursor mass tolerance; 1.0 Da product ion mass tolerance; full tryptic digestion; up to 3 missed cleavages; variable modification: oxidation of methionine (+15.9949), and carboxyamidomethylation (+57.0214637236) on cysteines; static modifications: TMTpro (+304.2071) on lysine and peptide N terminus. False discovery rate (FDR) was controlled to <1% on peptide level. Peptides that are shorter than seven amino acids were discarded. Site localization was determined using the ModScore (AScore) algorithm.[41] TMT reporter ion signal to noise ratios were used for quantification of peptide abundance.

QUANTIFICATION AND STATISTICAL ANALYSIS

Statistical significance was determined by two-way ANOVA or one-way ANOVA with Dunnet's or Tukey's post-hoc testing using GraphPad Prism software. Statistical details for each experiment (including statistical test used, value and definition of n, definition of center and dispersion/precision measures) can be found in the figure legends.